# Computational Fluid Dynamics and Interactive Multiobjective Optimization in Development of Low Emission Industrial Boilers

Ari Saario, Antti Oksanen




# Computational Fluid Dynamics and Interactive Multiobjective Optimization in Development of Low Emission Industrial Boilers

| | |
|---|---|
| Journal: | *Engineering Optimization* |
| Manuscript ID: | GENO-2007-0038.R2 |
| Manuscript Type: | Original Article |
| Date Submitted by the Author: | 06-Mar-2008 |
| Complete List of Authors: | Saario, Ari; Tampere University of Technology, Institute of Enegy and Process Engineering<br>Oksanen, Antti; Tampere University of Technology, Institute of Energy and Process Engineering |
| Keywords: | CFD, multiobjective optimization, interactive reference-point method, SNCR, NO emission |
| | |

Note: The following files were submitted by the author for peer review, but cannot be converted to PDF. You must view these files (e.g. movies) online.

Optimization_CFD.tex
Abstract
Introduction
Case_Description
Fluidized_Bed_Boiler
Selective_Noncatalytic_Reduction
Mathematical_Modeling
Optimization
Optimization_Problem
Multi_Objective_Optimization
Interactive_Multi_Objective_Optimization
Optimization_Algorithms
Genetic_Algorithm

# Computational fluid dynamics and interactive multiobjective optimization in development of low-emission industrial boilers

A. Saario*, A. Oksanen

Institute of Energy and Process Engineering, Tampere University of Technology,

Korkeakoulunkatu 6, P.O.Box 589, 33101 Tampere, Finland



## Abstract

A CFD-based model is applied to study emission formation in a bubbling fluidized bed boiler burning biomass. After the model is validated to a certain extent, it is used for optimization. There are nine design variables (nine distinct $NH_3$ injections in the selective noncatalytic reduction process) and two objective functions (minimize NO and $NH_3$ emissions in flue gas). The multiobjective optimization problem is solved using the reference-point method involving an achievement scalarizing function. The interactive reference-point method is applied to generate Pareto optimal solutions. Two inherently different optimization algorithms, viz. a genetic algorithm and Powell's conjugate direction method, are applied in the solution of the resulting optimization problem. It is shown that optimization connected with CFD is a promising design tool for combustion optimization. The strengths and weaknesses of the proposed approach and of the methods applied are discussed from the point of view of a complex real-world optimization problem.

Keywords: CFD, multiobjective optimization, interactive reference-point method, SNCR, NO emission.

*To whom correspondence should be addressed. Phone: +358 40 849 0879. Fax: +358 3 3115 3751. E-mail: ari.saario@tut.fi.

# 1 Introduction

The combination of computational fluid dynamics (CFD) and optimization has been commonly applied in some fields of engineering, such as in the development of aircraft (see e.g. Giannakoglou 2001) and of other means of transport (see e.g. Poloni *et al.* 2000), and to some extent e.g. in papermaking (see e.g. Hämäläinen *et al.* 1999). In contrast, the development of stationary combustion systems with CFD has typically not been based on a systematic search for the optimum. Rather, CFD has been used to calculate only few predefined cases chosen intuitively (or randomly) by the CFD user, after which the best result found has been frequently referred to as the "optimum solution".

Some examples of single-objective optimization (SOO) without CFD in the combustion-related problems follow. Zhou *et al.* (2001) minimized the NO emission of a coal-fired boiler. Homma and Chen (2000) minimized $NO_2$ emission in postflame processes. Kalogirou (2003) and Ward *et al.* (2006) provided a review of artificial intelligence techniques (including optimization) in combustion engineering. The application of both SOO and CFD in combustion-related problems is less common. Johnson *et al.* (2001) minimized the CO emission of a burner and Saario *et al.* (2006) minimized the NO emission of a fluidized bed boiler.

In most practical problems there are more than just one criterion to be optimized, and often these criteria conflict with each other. The simultaneous minimization of bubbling fluidized bed boiler NO and $NH_3$ emissions in the present study is a good example of such a multiobjective optimization (MOO) problem. Studies dealing with MOO without CFD in combustion-related problems are reviewed briefly. Chu *et al.* (2003) minimized the NO and CO emissions and maximized the thermal efficiency of a coal-fired boiler. Zhou *et al.* (2005) minimized the NO and unburned carbon emissions of a coal-fired boiler. Chen *et al.* (2003) minimized the NO emission and maximized the thermal efficiency of an engine. Also the optimization of simplified chemical reaction mechanisms can be considered as an MOO problem (Elliot *et al.* 2004, Montgomery *et al.* 2006, Polifke *et al.* 1998). There are only few examples of the application of both MOO and CFD in combustion-related problems (excluding aerospace applications). Risio *et al.* (2005) minimized the NO and unburned carbon emissions of two coal-fired boilers and Tan *et al.* (2006) minimized the NO, CO and unburned carbon emissions from the co-combustion of coal and biomass in a pilot-scale combustion rig. Again, also the optimization of temperature distribution in a burner (Catalano *et al.* 2006) or on a cooking surface (Bryden *et al.* 2003) can be considered as an MOO problem.

The decision maker is a person who is supposed to have better insight into the problem and who can express preference relations between different solutions (Miettinen 1999 p. 14). Usually, the decision maker is responsible for the final solution. In interactive multiobjective optimization methods, preferences of a decision maker are taken into account during the optimization process. It seems that interactive MOO methods have never been used in combustion-related problems previously.

# 2 Case description

The emission formation is studied in a bubbling fluidized bed (BFB) boiler which applies the selective noncatalytic reduction (SNCR) process to reduce the NO emission in flue gas.

## 2.1 *Bubbling fluidized bed (BFB) boiler*

Fluidized bed combustion is an advanced technology suitable for burning difficult (high moisture and ash content) fuels and fuel mixtures with low emissions (see e.g. Basu 2006). In a BFB boiler the velocity of fluidization air is low enough to keep the bed particles and other solids mainly in the bottom area of the boiler (out of the freeboard area). Today, modern BFB boilers in the pulp and paper industry have typical capacities of 40–300 $MW_{th}$. The air-staging may consist of up to three air injection levels, and the cross-sectional area and the height of the boiler may be up to 140 $m^2$ and 40 m, respectively.

A sketch of the BFB boiler studied here is shown in figure 1. The mixture burned in the boiler consists mainly of biomass sludge originating from the de-inking process and the effluent treatment plant of the newsprint mill. In addition, a moderate amount of plastic reject is mixed with the biomass sludge, and some natural gas ($CH_4$) is added into the boiler as supporting fuel. The boiler has a capacity of 40 $MW_{th}$. For the information on the chemical properties of the sludge and on the operating conditions of the boiler, see Saario and Oksanen (2008a).

## 2.2 *Selective noncatalytic reduction (SNCR)*

The SNCR process ($NH_3$ injection) is a low-cost, effective and retrofittable NO control strategy. The injected $NH_3$ initiates a sequence of reactions that converts NO formed in the lower part of the boiler into harmless $N_2$. The efficiency of NO reduction, the operating temperature and the $NH_3$/NO molar ratio in the SNCR process vary typically in the range 30–80%, 1073–1373 K, and 0.8–2.5, respectively (Radojevic 1998). The principal chemical reactions taking place in the SNCR process can be found in Miller and Bowman (1989).

The NO reduction efficiencies in practical combustion devices are primarily dependent on the following factors: absolute temperature level and nonisothermal temperature profile, local flue gas conditions, mixing of $NH_3$ and NO, $NH_3$/NO molar ratio and $NH_3$ residence time. The reduction of NO is achieved only inside a relatively narrow temperature window centred approximately at 1250 K. The presence of additives, such as CO, shifts the optimal temperature window towards lower temperatures. At too-high temperatures, $NH_3$ oxidizes to NO, while at too-low temperatures, $NH_3$ passes unreacted through the reaction zone, causing $NH_3$ emission (ammonia slip) in flue gas. The presence of $O_2$ is necessary for NO reduction by $NH_3$. Typically, industrial boilers have large cross-sectional areas over which the injection system must disperse $NH_3$ and mix it with NO. Moreover, these boilers may have to operate with different loads, which may change the spatial location of the optimal temperature window.

In the present study a mixture of $NH_3$ and air (the bulk of the mixture consists of air) is injected from two separate levels at heights of 6.5 m and 7.5 m (see

figure 1). There are eight injections at a height of 7.5 m (see figure 2) and one injection at a height of 6.5 m on the rear wall.

# 3 Mathematical modelling

A commercial finite-volume-based CFD solver Fluent (2005) is used to model boiler operation. Assuming variable-density steady-state flow, the Favre-averaged (see e.g. Poinsot and Veynante 2005) continuity and momentum equations can be written as

$$\frac{\partial}{\partial x_i}\left(\overline{\rho}\widetilde{u}_i\right) = 0 \tag{1}$$

$$\frac{\partial}{\partial x_j}\left(\overline{\rho}\widetilde{u}_j\widetilde{u}_i\right) = -\frac{\partial \overline{p}}{\partial x_i} + \frac{\partial}{\partial x_j}\left[\mu\left(\frac{\partial \widetilde{u}_i}{\partial x_j} + \frac{\partial \widetilde{u}_j}{\partial x_i} - \frac{2}{3}\delta_{ij}\frac{\partial \widetilde{u}_l}{\partial x_l}\right)\right] + \overline{\rho}g_i + \frac{\partial}{\partial x_j}\left(-\overline{\rho}\widetilde{u_i''u_j''}\right) \tag{2}$$

where $\rho$ is density, $u_i$ is the $i^{\text{th}}$ component of the velocity vector, $p$ is pressure, $\delta_{ij}$ is the Kronecker delta, $g_i$ is the $i^{\text{th}}$ component of the gravitational vector and $-\overline{\rho}\widetilde{u_i''u_j''}$ is the component of the Reynolds stress tensor. The overbar denotes time-averaging, the tilde denotes Favre-averaging and the double prime denotes the Favre-averaged fluctuating part. Here, the Reynolds stresses, $-\overline{\rho}\widetilde{u_i''u_j''}$, are modelled using a modification of the widely applied standard $k$-$\varepsilon$ model (Shih *et al.* 1995).

The boiler CFD modelling requires a conservation equation also for energy and equations for the species transport. The reactions of hydrocarbon species are modelled using the global mechanism of Jones and Lindstedt (1988). The turbulence-chemistry interaction of the hydrocarbon species is modelled using the simple eddy dissipation combustion model of Magnussen and Hjertager (1976) supplemented with an additional term to take into account the finite-rate chemistry. The reactions of the nitrogen-containing species ($NH_3$, NO) are modelled using a combination of the global mechanisms of Duo *et al.* (1992) and Brink *et al.* (2001). The turbulence-chemistry interaction of the nitrogen-containing species is modelled using the advanced eddy dissipation concept of Magnussen (Ertesvåg and Magnussen 2000). The low concentrations of NO and $NH_3$ are assumed not to affect significantly the distributions of velocity, density, temperature and other species (those not containing nitrogen). Hence, the postprocessing technique is applied to solve the transport equations of NO and $NH_3$, which speeds up the solution and is consequently a great advantage in the optimization stage. The radiative heat transfer equation is solved using the finite-volume method (Raithby and Chui 1990) and the gas-phase absorption coefficient is determined using the weighted-sum-of-grey-gases model of Smith *et al.* (1982). The boundary conditions on the bed surface are obtained on the basis of element and energy balances of the known fuel composition. These balances are supplemented by laboratory experiments and by reasonable assumptions regarding fuel supply and bed processes.

On the basis of a thorough grid-refinement study, here a structured grid consisting of 348 709 computational cells is built. The grid is refined locally twice

in the vicinity of the $NH_3$ injections using velocity gradients as the refinement criterion. In both refinement steps the number of cells is increased on average by 3444 per each $NH_3$ injection. The number of cells at the $NH_3$ injection inlets varies between 40 and 52.

A detailed description of the grid-refinement study, numerical solution procedure and turbulence modeling, and of the issues related to the reactive-flow modeling and to the definition of bed boundary conditions in the present study can be found in Saario and Oksanen (2008b, 2008a).

# 4 Optimization

In an earlier study (Saario *et al.* 2006) it was shown that the boiler NO emission can be decreased significantly using the optimization. However, the same study revealed that single-objective optimization (SOO) is not sufficient in the SNCR process optimization, since a low NO emission was achieved at the expense of a high $NH_3$ emission. In the present study, multiobjective optimization (MOO), where the number of objectives is greater than one, must be applied if results of practical use are desired.

## 4.1 *Optimization problem*

Here, the aim is to minimize both NO and $NH_3$ concentrations in flue gas. There are altogether nine independent design variables, each corresponding to the $NH_3$ mole fraction of a distinct injection. In other words, the distribution of $NH_3$ between the injections, as well as the total amount of $NH_3$ injected into the boiler, are varied in the optimization. The maximum total amount of $NH_3$ available for the injections is limited by the capacity of the $NH_3$ feeding system. The resulting inequality constraint is incorporated into the optimization problem using a penalty function method. Furthermore, the limits inside which the design variables are allowed to vary (design variable bounds) are specified. A mathematical formulation of the present optimization problem is given in the following section 4.2.

## 4.2 *Multiobjective optimization*

The general definition of multiobjective optimization problem is

$$\underset{\boldsymbol{x}\in S}{\text{minimize}}\ \boldsymbol{f}\left(\boldsymbol{x}\right) = \left(f_1\left(\boldsymbol{x}\right), f_2\left(\boldsymbol{x}\right), \ldots, f_m\left(\boldsymbol{x}\right)\right)^{\mathrm{T}} \tag{3}$$

where $\boldsymbol{f}\left(\boldsymbol{x}\right)$ is an objective function vector and $m$ $(\geq 2)$ is the number of objective functions $f_i$: $\mathbb{R}^n \rightarrow \mathbb{R}$ for all $i \in \{1, \ldots, m\}$. The design variable vector, $\boldsymbol{x}$, is given by

$$\boldsymbol{x} = \left(x_1, x_2, \ldots, x_n\right)^{\mathrm{T}} \tag{4}$$

where $n$ is the number of design variables. Design variable vector $\boldsymbol{x}$ belongs to the feasible set, $S$, defined as

$$S = \left\{\boldsymbol{x} \in \mathbb{R}^n \mid \boldsymbol{x}^{\mathrm{l}} \leq \boldsymbol{x} \leq \boldsymbol{x}^{\mathrm{u}},\ \boldsymbol{g}\left(\boldsymbol{x}\right) \leq \boldsymbol{0},\ \boldsymbol{h}\left(\boldsymbol{x}\right) = \boldsymbol{0}\right\} \tag{5}$$

where $\boldsymbol{x}^{\mathrm{l}}$ and $\boldsymbol{x}^{\mathrm{u}}$ denote lower and upper design variable bounds, respectively, $\boldsymbol{g}(\boldsymbol{x})$ is a vector of inequality constraints, and $\boldsymbol{h}(\boldsymbol{x})$ is a vector of equality constraints. For any design variable vector $\boldsymbol{x} \in \mathbb{R}^n$, a corresponding image vector $\boldsymbol{f}(\boldsymbol{x}) \in \mathbb{R}^m$ in the objective space is obtained using mapping $\boldsymbol{f}$: $\mathbb{R}^n \rightarrow \mathbb{R}^m$.

The design variable vector $\boldsymbol{x}^* \in S$ is Pareto optimal if and only if there does not exist another vector $\boldsymbol{x} \in S$ which satisfies the conditions (minimization problem assumed):

$$\begin{aligned} &f_i(\boldsymbol{x}) \leq f_i(\boldsymbol{x}^*) \text{ for all } i \in \{1, \ldots, m\} \text{ and} \\ &f_i(\boldsymbol{x}) < f_i(\boldsymbol{x}^*) \text{ for at least one } i \in \{1, \ldots, m\} \end{aligned} \tag{6}$$

A feasible vector is weakly Pareto optimal if there is no other feasible vector that decreases all of the objective functions simultaneously.

Objective function vector $\boldsymbol{f}(\boldsymbol{x})$ is given in the present study by

$$\boldsymbol{f}(\boldsymbol{x}) = (f_1(\boldsymbol{x}), f_2(\boldsymbol{x}))^{\mathrm{T}} \tag{7}$$

where $f_1(\boldsymbol{x})$ and $f_2(\boldsymbol{x})$ measure the concentrations of NO and $NH_3$ ($ppm_{vol}$) in flue gas, respectively. The design variable vector, $\boldsymbol{x}$, is given by

$$\boldsymbol{x} = (X_1, X_2, \ldots, X_9)^{\mathrm{T}} \tag{8}$$

where $X_i$ stands for the concentration of $NH_3$ (vol-%) in the $i^{\mathrm{th}}$ injection port. The feasible set, $S$, is defined as

$$S = \left\{ \boldsymbol{x} \in \mathbb{R}^n \mid 0 \leq X_i \leq 6.60 \text{ for all } i \in \{1, 2, \ldots, 9\}, \right. \\ \left. g(\boldsymbol{x}) = \dot{m}_{\mathrm{flow}} \frac{M_{\mathrm{NH_3}}}{M_{\mathrm{flow}}} \sum_{i=1}^{9} X_i - \dot{m}_{\mathrm{NH_3,max}} \leq 0 \right\} \tag{9}$$

The upper design variable bounds are set at 6.60 vol-% for all $i \in \{1, 2, \ldots, 9\}$. This value is based on the preliminary optimization studies and engineering intuition. If design variable bounds were too large, much of the search time would be wasted in exploring regions far from the feasible set, whereas too tight bounds might not allow finding the optimum. In the preliminary studies, where the upper design variable bounds were set at values smaller than 6.60, some design variables reached the upper bounds at the optimum solution. Hence, here the upper bounds were increased to 6.60, which correspond to the values at the current operating point multiplied by ten ($X_i = 0.66$ vol-% for all $i \in \{1, 2, \ldots, 9\}$ at the current operating point). Constraint $g(\boldsymbol{x})$ is an inequality constraint, $M$ is the molar mass ($M_{\mathrm{NH3}} = 17.03$ kg kmol$^{-1}$ and $M_{\mathrm{flow}} = 28.77$ kg kmol$^{-1}$) and $\dot{m}_{\mathrm{flow}}$ stands for the total mass flow of the mixture of $NH_3$ and air from a single injection ($\dot{m}_{\mathrm{flow}} = 0.1313$ kg s$^{-1}$). Symbol $\dot{m}_{\mathrm{NH_3,max}}$ stands for the maximum total amount of $NH_3$ that can be injected into the boiler. It is set at 0.0093 $\mathrm{kg_{NH_3}}$ s$^{-1}$, which corresponds to double the total $NH_3$ mass flow injected into the boiler at the current operating point.

The weighting method, where a weighted sum of the objective functions is optimized, is one of the oldest approaches to the solution of MOO problems (Cohon

1978) and it has been by far the most popular approach in combustion-related MOO studies (Bryden *et al.* 2003, Catalano *et al.* 2006, Chen *et al.* 2003, Chu *et al.* 2003, Elliot *et al.* 2004, Montgomery *et al.* 2006, Polifke *et al.* 1998, Risio *et al.* 2005, Tan *et al.* 2006), probably because it is intuitive to the user. However, in some of the studies the weighting method has been applied probably without actually realizing that an MOO problem is being dealt with. In the weighting method it is impossible to obtain points in a nonconvex portion of the Pareto set in the objective space (Das and Dennis 1997, Koski 1985, Marler and Arora 2004, Miettinen 1999). Moreover, specifying the weights is not straightforward. An even spread of weights does not guarantee an even spread of points in the Pareto set in the objective space (Cohon 1978, Das and Dennis 1997).

Instead of the weighting method, here the MOO problem is converted into a single-objective optimization problem using the achievement scalarizing function introduced by Wierzbicki (see Miettinen (1999 pp. 107–112) and Wierzbicki (1982)), which overcomes the typical disadvantages of the weighting method discussed above. An achievement scalarizing function (in the following shortened to achievement function) is a function satisfying certain requirements and the form applied here is closely related to the Tchebycheff distance metric (min-max formulation).

A few definitions are needed at this point. A vector (or "point" or "solution") consisting of the objective function values that are desirable or reasonable to the decision maker is called a reference point $\boldsymbol{z}^{\mathrm{ref}}$. An ideal objective vector $\boldsymbol{z}^{\mathrm{id}}$ is obtained by minimizing each of the objective functions individually subject to constraints (see figure 3). A vector consisting of the maximum objective function values in the Pareto set is called a nadir objective vector $\boldsymbol{z}^{\mathrm{nad}}$ (see figure 3). Vectors $\boldsymbol{z}^{\mathrm{id}}$ and $\boldsymbol{z}^{\mathrm{nad}}$ are used here to normalize the objective functions so that their objective values are approximately of the same order of magnitude. Here, the optimization problem is formulated as

$$\underset{\boldsymbol{x}\in S'}{\text{minimize}} \left( \max_{i=1,2} \left( \frac{f_i(\boldsymbol{x}) - z_i^{\mathrm{ref}}}{z_i^{\mathrm{nad}} - z_i^{\mathrm{id}}} \right) + \rho \sum_{i=1}^{2} \left( \frac{f_i(\boldsymbol{x}) - z_i^{\mathrm{ref}}}{z_i^{\mathrm{nad}} - z_i^{\mathrm{id}}} \right) + r \left[ \max\left(0, g(\boldsymbol{x})\right) \right]^2 \right) \tag{10}$$

The first term in equation (10) is the achievement function which projects the reference point vector $\boldsymbol{z}^{\mathrm{ref}}$ onto the Pareto optimal set. The second term is the normalized augmentation term, which prevents from generating solutions that are only weakly Pareto optimal (for details see Miettinen (1999 pp. 100–102)). The third term is the quadratic exterior penalty function, which penalizes infeasible solutions and becomes more severe with increasing distance from feasibility. The augmentation coefficient, $\rho$, is set at 0.0001, and the penalty parameter, $r$, is set at 20 000. Feasible set $S'$ includes the upper and lower design variable bounds but not inequality constraint $g(\boldsymbol{x})$ which is included in the function to be minimized. The solution of the optimization problem in equation (10), i.e. the solution of the achievement function including an augmentation term, is properly Pareto optimal (Miettinen 1999, Wierzbicki 1982).

### 4.3 *Interactive multiobjective optimization*

Let us define two concepts following Miettinen (1999 p. 14). A decision maker (DM) is a person who is supposed to have better insight into the problem and who can express preference relations between different solutions. An analyst is a person or computer program responsible for the mathematical side of the solution process. The analyst generates information for the DM and the solution is sought and selected according to the preferences of the DM. In interactive methods the DM and the analyst communicate and analyze the obtained solutions and their interactions during the optimization. Only some of the Pareto optimal solutions are generated, which is a considerable advantage considering the great amount of computing time required in CFD modeling.

Here, Pareto optimal solutions are generated using the interactive reference-point method of Wierzbicki (see Miettinen (1999 pp. 164–170) and Wierzbicki (1982)) utilizing an achievement-function-based problem. The DM expresses his/her preferences in the form of a reference point, which is a point desirable or reasonable to him/her. The reference point can be a feasible or infeasible point in the objective space. When the objective function values (reference points) are used, problems can be dealt with naturally on their own terms and there is no necessity to artificially specify e.g. monetary values or weighting coefficients for all the objectives.

The interactive algorithm works as follows. To start, some initial information may be given to the DM (here, $\boldsymbol{z}^{\mathrm{id}}$ and $\boldsymbol{z}^{\mathrm{nad}}$ were given), after which the DM sets the first reference point. Then, the analyst generates the Pareto-optimal solution(s) corresponding to the reference point (in other words the analyst projects the reference point(s) onto the Pareto set) and shows the solution to the DM. If the DM is satisfied with the solution obtained, the algorithm stops; otherwise, the DM sets a new reference point and the interactive procedure is repeated. Due to the great amount of computing time required in generating Pareto optimal solutions, here only one Pareto optimal solution is generated for the DM in each interactive step (a new step begins after the specification of a new reference point). The original method suggests generating several Pareto optimal solutions for the DM in each interactive step, using the so-called perturbed reference points (Wierzbicki 1982 pp. 402–403).

### 4.4 *Optimization algorithms*

Two fundamentally different optimization algorithms, viz. a genetic algorithm and Powell's conjugate direction method, are applied in the present study to solve the optimization problem given in equation (10). Both of them are zero-order methods, indicating that information on gradients is not required. Here, a hybrid optimizer is used to exploit the benefits of the two different algorithms; a GA run consisting of 600 CFD evaluations is performed first (global search), after which the search is continued from the solution found, using Powell's conjugate direction method (local search).

#### 4.4.1 *Genetic algorithm*

Genetic algorithms (GA) are based on the concepts of natural selection and the survival of the fittest. GAs converge towards the global solution rather than towards a local solution, and they are robust and easy to use. GAs use a stochastic population-based approach, in which several search points exist simultaneously.

Several possible variations of a GA exist. Hence, when defining a GA, one needs to choose its components, such as representation, selection mechanism, crossover and mutation operators and an initial population. These components may have parameters, such as the tournament size in tournament selection, the probabilities of crossover and mutation and the population size.

The principle of the GA and the main parameters applied in the present study are shown in figure 4. The effects of population size and mutation probability on the GA convergence rate were studied. In these studies, each GA run with a certain parameter set was repeated five times using different random seeds and the average performance of these five runs was used to evaluate the convergence rate. It was observed that the population size 10 converges clearly at a faster rate than the population size 50. In contrast, the convergence rate between the mutation probabilities 0.01 and 0.10 does not differ significantly. On the basis of these findings, the population size is set at 10 and the mutation probability is set at 0.10.

Each continuous design variable $X_i$ is represented using the binary representation of six digits and applying Gray binary coding. The resulting set of 64 discrete search points has an accuracy of 0.1 vol-% in the design space. A GA of commercial software for evolutionary optimization EASY (Giannakoglou and Giotis 2007) is applied. For a more detailed description of GAs, see e.g. Osyczka (2002).

#### 4.4.2 *Powell's conjugate direction method*

Powell's conjugate direction method (Powell 1964) (in the following shortened to Powell's method) is an effective and widely used method and it is described in detail e.g. in Belegundu and Chandrupatla (1999). Unlike a GA, Powell's method improves a single search point in an iterative manner by employing deterministic rules. Deterministic methods are effective in finding a local optimum, but are not well suited for global optimization because the final solution may depend on the starting point.

Figure 5 shows the principle of Powell's method. First, the objective function $f$ is minimized along each of the $n$ (number of design variables) coordinate directions in turn, followed by another minimization along the first direction (minimization problem assumed). Every minimization is started from the best point found so far. In each search direction, the minimum is bracketed inside a certain interval, after which a quadratic-fit golden-section algorithm (Chandrupatla 1998) is applied for the one-dimensional step length optimization. Second, a linearly independent conjugate direction, which lies in the general direction of the minimum, is generated. The conjugate direction, $\boldsymbol{s}_i$, is defined as

$$\boldsymbol{s}_i = \boldsymbol{x}_i - \boldsymbol{x}_{i-n} \tag{11}$$

where $\boldsymbol{x}_i$ is the point obtained at the end of $n$ one-dimensional minimization steps and $\boldsymbol{x}_{i-n}$ is the point before taking the $n$ steps. Then, one of the $n$ coordinate directions is discarded in favour of the generated conjugate direction. After that, the minimization is repeated along each of the remaining $n$ directions, using the generated conjugate direction as the first direction. Then, a new conjugate direction is generated and the loop is repeated, until the minimization has been performed along all $n$ conjugate directions. Finally, unless the stopping criterion (the change in $f$ less than a specified amount with respect to the starting values) is met, the whole algorithm re-starts from the beginning by minimizing along the coordinate directions.

Here, the computational cost related to Powell's method is relatively low. In general, the most significant progress is made during the first 20 CFD evaluations and after 90 CFD evaluations only negligible improvements are obtained. Although not shown here, the performance of Powell's method proves to be strongly dependent on the starting point if applied as the only optimization algorithm in the present case. Hence, the objective space in the present study is not simple but contains several local optima.

# 5 Results and discussion

First, the model validation carried out before the optimization is described briefly. Then, the Pareto optimal solutions and the interactive reference-point method used to generate them are discussed. After this, the final solution is selected and some observations are made on the consistency between the Pareto optimal solutions and the known physical behaviour of the SNCR process. Finally, the optimization results are evaluated by comparing them with the available experimental data.

Computations were performed using a 2.2 GHz AMD Opteron processor. A single function evaluation took one hour. Approximately 700 function evaluations were required to obtain a single Pareto optimal solution. In other words, approximately one month was required for generating each Pareto optimal solution.

## 5.1 *Model validation*

Today, a CFD-based study of a real-world combustion device contains necessarily significant uncertainties. The computational grid and numerical solution procedure, as well as several submodels, affect the accuracy of CFD modelling. It is obvious that the capability of CFD to give qualitatively correct predictions is a prerequisite for the application of optimization.

The overall CFD model is validated using the experimental data and sensitivity studies (see Saario and Oksanen 2008a, 2008b). First, a thorough grid-refinement study was carried out before creating the computational grid applied here. Then, several global ammonia chemistry mechanisms were compared and suitable mechanisms were identified for the conditions in the present study. Finally, the model predictions were validated to a certain extent against the experimental data obtained in the full-scale bubbling fluidized bed boiler.

## 5.2 *Pareto optimal points*

The optimization problem in equation (10) is solved by applying the hybrid optimizer. First, five GA runs are performed using different random seeds (each GA run consists of 600 function evaluations), after which Powell's method is started from the best GA solution found. The interactive reference-point method is used to generate the Pareto optimal solutions. Strictly speaking, some points termed here "Pareto optimal" may not be exactly such, since the number of function evaluations available was limited. When discussing Pareto optima, the terms "point" and "solution" will be used interchangeably.

Figure 6 shows the predicted current design point, four predicted points from the Pareto optimal set and two reference points in the objective space. The point "Current design" refers to the currently used operating point, in which $X_i = 0.66$ vol-% for all $i \in \{1, 2, \ldots, 9\}$ in the design space. As shown in figure 6, the corresponding prediction in the objective space is $\boldsymbol{f}(\boldsymbol{x}) = (f_{\mathrm{NO}}(\boldsymbol{x}), f_{\mathrm{NH3}}(\boldsymbol{x})) = (75.4, 7.7)$. The current design seems relatively good, which is not surprising when one considers that it is the result of the experience and years of work of engineers.

The point "SOO NO" is obtained from the solution of a single-objective optimization problem. The point "SOO NH3" is obtained by solving a single case (all $NH_3$ injections turned off), which was specified by applying reasoning and knowledge of the process. After solving the end points of the Pareto set in the objective space, $\boldsymbol{z}^{\mathrm{id}}$ can be determined as $\boldsymbol{z}^{\mathrm{id}} = (z^{\mathrm{id}}_{\mathrm{NO}}, z^{\mathrm{id}}_{\mathrm{NH_3}}) = (53.1, 0.0)$. Then, $\boldsymbol{z}^{\mathrm{nad}}$ is obtained from the payoff table (see Miettinen (1999, pp. 16–18)), which yields $\boldsymbol{z}^{\mathrm{nad}} = (z^{\mathrm{nad}}_{\mathrm{NO}}, z^{\mathrm{nad}}_{\mathrm{NH_3}}) = (108.2, 47.5)$. Points "MOO I" and "MOO II" refer to the solutions of the MOO problem using reference points ($\boldsymbol{z}^{\mathrm{ref}}$ in equation (10)) "Reference point I" and "Reference point II", respectively.

As mentioned earlier, the minimum $NH_3$ emission is obtained by turning off all the $NH_3$ injections. Figure 7 shows the design variables corresponding to the other three Pareto optima shown in figure 6. As expected, to minimize the NO emission only, plenty of $NH_3$ should be injected (see figure 7(a)). The inequality constraint limiting the maximum total amount of $NH_3$ that can be injected (see equation (9)) is violated only in the solution of the "SOO NO" case. In general, the design variables are far from the upper design variable bounds. However, injection "Side left C" in the "SOO NO" case hits the upper design variable bound, and hence still greater values of the upper bounds than 6.60 set in equation (9) could have been used. Figure 7 shows also that when both objectives are considered, $NH_3$ is more evenly distributed between the injections than in the "SOO NO" case.

In order to make sure that the algorithm found at least a local optimum, additional calculations were performed in the surroundings of points "SOO NO", "MOO I", and "MOO II". These calculations were performed by increasing and decreasing each design variable, one at a time, using a small step size $\Delta X_i$. On the basis of additional calculations, all the points seem to be (locally) optimal inside $\Delta X_i = \pm 0.2$ vol-% for all $i \in \{1, 2, \ldots, 9\}$ in the design space.

## 5.3 *Interactive reference-point method*

The interactive reference-point method is applied to generate Pareto optimal solutions. In the present study the role of decision maker (DM) is undertaken

by two research engineers from a boiler manufacturing company. After some negotiations and exchange of views, the DMs reached unanimous decisions easily. Thus, we have a unanimous group of two DMs. It is probable that some persons involved in the real decision-making process are left out here because they are not easily accessible, or perhaps because they have not been identified at all. One should note that other decision makers would probably have somewhat different preferences, or perhaps even different objectives, but this is characteristic of MOO, where typically no absolute optima exist.

In general, interactive methods make it possible to obtain a satisfactory solution with a reasonable number of function evaluations, which is important in the present study due to the great amount of computing time required in generating Pareto optimal points. The interactive reference-point method is found to be a good method. It is easy to understand for the DMs, since the DMs are required to supply information only in terms of the reference points. In the present study the reference points are the concentrations of NO and $NH_3$ in flue gas, which are concepts familiar to the DMs. When requesting reference-point information from the DMs, it was found important to use units that the DMs are accustomed to use. In the decision-making meetings the objective function values were presented to the DMs in $\mathrm{mg_{NO2}\ Nm^{-3}}$ at 11% $O_2$ (dry) and in $\mathrm{mg_{NH3}\ Nm^{-3}}$ at 11% $O_2$ (dry), although here the results are presented in $\mathrm{ppm_{vol}}$.

The end points of the Pareto set in the objective space ("SOO NO" and "SOO NH3") provide important information for the DMs. All the information was presented to the DMs both in the objective and design space. The DMs appreciated seeing all the information available before specifying a reference point. They appreciated also having received the information available already a few days before the actual decision-making meeting. The interest and commitment of the DMs, and possibly also their understanding of the problem, are increased when the interactive method is applied.

Negative features of interactive methods include the extra time required for the decision-making meetings. Moreover, some interactive methods found in the literature are probably too demanding for real-world DMs. Here, the time between the successive decision-making meetings was more than one month due to the great amount of computing time, which makes the application of interactive methods less attractive. Also, the specification of a reference point was found to be somewhat confusing at a certain stage, since the known experimental points did not always agree well enough with the results of the mathematical model (especially with very high or low ammonia injection settings). This issue is related to the model validation and it is discussed further in section 5.6. The interactive methods would show their strength probably more clearly if the number of objectives were greater than two, although the possibilities to visualize the results for the DMs would be significantly weakened.

To start, the analyst generated ideal and nadir points, after which "Reference point I" was set to correspond to the ideal point as $\boldsymbol{z}^{\mathrm{refI}} = (z_{\mathrm{NO}}^{\mathrm{refI}}, z_{\mathrm{NH_3}}^{\mathrm{refI}}) = (53.1, 0.0)$. Then, the analyst generated Pareto point "MOO I", after which the DMs set "Reference point II" at $\boldsymbol{z}^{\mathrm{refII}} = (z_{\mathrm{NO}}^{\mathrm{refII}}, z_{\mathrm{NH_3}}^{\mathrm{refII}}) = (56.9, 15.4)$. The two reference points are shown in figure 6. Here, a satisfactory solution was found after two interactive steps.

During the search for Pareto optimal solutions, a great number of function

evaluations is performed. Every function evaluation produces one point, many of which are not guaranteed to be Pareto optimal, but can nevertheless be useful. Hence, these points should not be discarded, as they may provide important information to the DMs or possibly include even the final solution. Here, altogether about 10 000 function evaluations were performed during cases "SOO NO", "MOO I", and "MOO II". Of these points, figure 8 shows all the feasible ones and the ones which exceed $\dot{m}_{\mathrm{NH_3,max}}$ at maximum by 5% ($\dot{m}_{\mathrm{NH_3,max}} = 0.0093\ \mathrm{kg_{NH3}\ s^{-1}}$, see $g(\boldsymbol{x})$ in equation (9)). The violation of 5% can be considered acceptable because $g(\boldsymbol{x})$ is a so-called soft constraint. Interestingly, after the second interactive step, the DMs were able to picture the whole Pareto set in the objective space in their mind quite reliably after having seen all the calculated points (see figure 8). In other words, it is found that the interactive MOO method applied may produce a reasonable approximation of the Pareto set in a computationally efficient manner.

It is pointed out that there exists another somewhat related approach, in which GAs are tailored to generate an approximation of the whole Pareto set within a single run of the algorithm (see e.g. Deb 2001, Fonseca and Fleming 2000 or Marler and Arora 2004). In this approach, individuals are ranked on the basis of whether or not they are dominated by other individuals. Then, the objective function value is assigned on the basis of the individuals' rank. To foster an even spread of points in the objective space, the value of the objective function of individuals in crowded areas is reduced, thus reducing the probability of their survival to the next generation.

Here, the reference-point method involving an achievement scalarizing function is applied to solve the MOO problem. However, since in the present study a suitable scaling has been used for the objective functions and the form of the approximated Pareto set is "non-surprising" (not a concave curve and not an excessively flat convex curve, as shown in figure 8), it is probable that also the weighting method would have yielded reasonable solutions here and that setting the weights would have been relatively easy.

## 5.4 *Selection of final solution*

Mathematically, every Pareto optimal point is an equally acceptable solution to an MOO problem. The selection of the final solution (also called best-compromise solution (Cohon 1978)) from among the obtained solutions is up to the decision makers (DMs), for whom some Pareto optimal solutions are preferable to some others. The approximated Pareto set in the objective space shown in figure 8 seems regular (almost convex) and there does not seem to be any "knees", which would obviously be preferable to the DMs.

Figure 9 shows an enlargement of the region between points "MOO I" and "MOO II" in the objective space, again including also the points which exceed $\dot{m}_{\mathrm{NH_3,max}}$ at maximum by 5%. This is the region the DMs found most attractive. In this region, the DMs' selection of the final solution is based on the guaranteed emission limit of $NH_3$ ($f_{2,\mathrm{guar}}(\boldsymbol{x}) = 15\ \mathrm{ppm_{vol}}$), which cannot be exceeded. The three white circles and the white star in figure 9 show four points which do not exceed the guaranteed limit and which the DMs find attractive. The solution to be implemented in the plant is selected from among these four options. The corresponding solutions in the design space are shown in figure 10. All

these solutions are far from the upper design variable bounds and the inequality constraint is not active or violated in any of them. It can be observed that the solutions which are close to each other in the objective space may differ significantly from each other in the design space.

Solution "a" in figure 9 is the best available choice which satisfies the guaranteed emission limit. However, the DMs prefer to have some safety margin to the guaranteed limit (from this point of view the solution marked with the star is the most tempting option). On the other hand, although the inequality constraint is not active or violated in any of the optional solutions, a lower $\dot{m}_{\mathrm{NH_3}}$ is preferred to a higher $\dot{m}_{\mathrm{NH_3}}$ by the DMs (from this point of view solution "c" is the most tempting option). After these considerations, the solution marked with the star in figure 9 is selected by the DMs as the final solution of the optimization problem.

In figure 11 the robustness of the final solution is evaluated to some extent by varying $X_9$ from the lower to the upper bound. Figure 11 illustrates also the functioning of the achievement function applied, which aims at reducing the NO emission when $X_9 < 0.21$ vol-%, otherwise it aims at reducing the $NH_3$ emission (see also equation (10)). Constraint $g(\boldsymbol{x})$ is violated when $X_9 \geq 3.14$ vol-%. The effect of penalty function can be seen as an increase in the slope of achievement function. Note also that the function to be minimized is nondifferentiable in the optimum.

With respect to the current operating point, the final solution yields approximately a 12% decrease in the NO emission while maintaining the $NH_3$ emission at an acceptable level. Finally, it must be emphasized here that in reality the implementation of the final solution requires care due to the significant uncertainties related to the mathematical modelling and the changing conditions in the real boiler.

### 5.5 *Consistency between Pareto optimal solutions and known physical behaviour of SNCR process*

Two common principles can be identified in the design variables of all the optional good solutions shown in figure 10. First, the amount of $NH_3$ injected from injection "Side left C" should be increased to 3–4 vol-%. Second, "Front left" injection should be turned almost off.

In the vicinity of injection "Side left C" the temperature is indeed suitable for NO reduction (see figure 12(a)). In contrast, in the vicinity of injection "Front left" there is a high temperature region which is known to enhance NO formation. Moreover, there is a considerable amount of CO (see figure 12(b)) and $H_2$ in the vicinity of injection "Front left", which is known to shift the optimal NO reduction temperature to a lower level. These findings suggest that $NH_3$ from injection "Front left" may form more NO instead of reducing it. On the other hand, figure 12(c) shows that there is little $O_2$ available (in a large region below 0.5 vol-%) in the vicinity of injection "Front left", which may partly limit NO formation regardless of the high temperature and the presence of CO and $H_2$.

It is difficult to specify with much certainty any general principles for the other injections. However, perhaps the amount of $NH_3$ from injections "Side left A" and "Side right B" should be decreased, and injections "Side right A" and "Side right C" should be kept unchanged.

In general, when comparing the "SOO NO" case in figure 7(a) with MOO cases in figures 7(b), 7(c) and 10, the findings suggest that the $NH_3$ injected should be more evenly distributed when both objectives are taken into account. Five injections are completely turned off in the solution of the "SOO NO" case shown in figure 7(a), which is probably due to the inequality constraint. Moreover, the great amount of $NH_3$ in injections "Side left C" and "Side right C" in the "SOO NO" case decreases in the MOO cases, because some of the $NH_3$ is likely to pass unreacted into flue gas due to the relatively low temperature in the vicinity of the rear wall.

Figure 12(d) shows the predicted NO concentration in the current design. The NO concentration is highest in the rear side of the cross-section. This supports the finding that more $NH_3$ should be injected from injection "Side left C". $NH_3$ is relatively well dispersed over the cross-section with the current injection arrangement (see figure 12(e)). The dispersion of $NH_3$ seems better in the right side of the cross-section. This effect is due to a strong downward flow in the vicinity of the right side wall injections, as shown in figure 12(f). A downward flow, although weaker, can be observed also in the vicinity of the left side wall injections. All in all, different injections encounter clearly different conditions inside the boiler. It may be difficult to identify the effect of interactions between the injections on the emissions in flue gas.

### 5.6 *Comparison with experimental data*

Some experimental data obtained from the bubbling fluidized bed boiler are available. The concentrations of NO and $NH_3$ in the flue-gas channel are measured with three different $NH_3$ injection settings (50%, 100% and 150% injection of $NH_3$ with respect to current operating point). The three experimental points and the corresponding CFD predictions are shown in figure 13. In addition, Pareto optimal solutions "SOO NO", "SOO NH3", "MOO I" and "MOO II" are included in figure 13.

The experimental data and predictions are in good agreement in the cases "50% injection" and "100% injection", whereas in the case "150% injection" there is a significant discrepancy. In fact, point "150% injection exp." in figure 13 suggests that predicted Pareto optimal solutions "SOO NO", "MOO I" and "MOO II" are not Pareto optimal in the actual practice. Although this inconsistency can be attributed partially to the significant experimental uncertainty, probably the deficiencies in the mathematical model are mainly responsible for it. In fact, it was found in Saario and Oksanen (2008a) that although the model predicts qualitative trends correctly, it is not capable of yielding correct quantitative results. In general, these findings show that it is important to validate any model at least to a certain extent before it can be used for optimization. Frequently, the application of modelling and optimization becomes an iterative loop.

## 6 Conclusions

A combination of computational fluid dynamics (CFD) and interactive multiobjective optimization is applied to find the optimal settings of nine $NH_3$ injections in order to minimize NO and $NH_3$ emissions from a real-world industrial boiler. With respect to the current design, approximately 12% decrease in the NO emission is obtained while maintaining the $NH_3$ emission at an acceptable level. In

the optimum solution, the amount of $NH_3$ varies strongly between $NH_3$ injections. In the present case, it is observed that the amount of $NH_3$ should be significantly increased from injection "Side left C" and decreased from injection "Front left".

The achievement scalarizing function is applied to convert the multiobjective optimization problem into a single-objective optimization problem. The converted single-objective optimization problem is solved using first a genetic algorithm for the exploration of design space and then Powell's conjugate direction method for local refinement near the optimum. This hybrid method is found to be an effective approach.

The interactive reference-point method is used to generate a satisfactory Pareto optimal solution at a relatively low computational cost. Interestingly, here an approximation of the Pareto optimal set is obtained as a "by-product" during interactive optimization. It is found important to apply an interactive method that requires information in a form easily understandable to the decision makers (DMs). Also, it is important to use units that the DMs are accustomed to use. The interest and commitment of the DMs, and possibly also their understanding of the problem, are increased when the interactive method is applied. The additional time required for the meetings between the DMs and the analyst can be considered as a disadvantage of interactive methods.

The experimental data obtained from the boiler emphasizes the fact that a model must be validated before it can be applied in optimization. In reality, the implementation of the optimal solution obtained here requires care due to the significant uncertainties related to the mathematical modelling and the changing conditions in the real boiler. Frequently, the application of modelling and optimization becomes an iterative loop.

In the near future, fast-growing computing capacity will enable wide-spread application of CFD-based optimization that typically requires a great number of expensive function evaluations. This efficient and scientific approach is easily applicable to many types of design and retrofit problems in combustion devices. Possible objectives include e.g. the minimization of various emissions, number of inlets, boiler corrosion, slagging and fouling, boiler size, temperature and velocity gradients, or costs, or they include the maximization of thermal efficiency or heat transfer. Possible design variables include e.g. the geometry, fuel feed, fuel quality, particle size distribution of fuel, air distribution system, swirl angle, injection of additives, or flue gas recirculation.

# Acknowledgments

The authors are greatly obliged to Prof. Juhani Koski from Tampere University of Technology and Prof. Kaisa Miettinen from the University of Jyväskylä for discussions. The participation of Mr. Matti Ylitalo and Mr. Juha Roppo as decision makers is gratefully acknowledged. The financial assistance from the Finnish Funding Agency for Technology and Innovation (Tekes) and Metso Power Oy is also thankfully acknowledged.

# References


Basu, P., *Combustion and Gasification in Fluidized Beds*, 2006 (Taylor & Francis: Boca Raton).

Belegundu, A.D. and Chandrupatla, T.R., *Optimization Concepts and Applications in Engineering*, 1999 (Prentice-Hall: New York).

Brink, A., Kilpinen, P. and Hupa, M., A simplified kinetic rate expression for describing the oxidation of volatile fuel-N in biomass combustion. *Energy & Fuels*, 2001, **15**, 1094–1099.

Bryden, K.M., Ashlock, D.A., McCorkle, D.S. and Urban, G.L., Optimization of heat transfer utilizing graph based evolutionary algorithms. *International Journal of Heat and Fluid Flow*, 2003, **24**, 267–277.

Catalano, L.A., Dadone, A., Manodoro, D. and Saponaro, A., Efficient design optimization of duct-burners for combined-cycle and cogenerative plants. *Engineering Optimization*, 2006, **38**, 801–820.

Chandrupatla, T.R., An efficient quadratic fit – sectioning algorithm for minimization without derivatives. *Computer Methods in Applied Mechanics and Engineering*, 1998, **152**, 211–217.

Chen, J-Y., Dibble, R.W., Kolbu, J. and Homma, R., Optimization of homogeneous charge compression ignition with genetic algorithms. *Combustion Science and Technology*, 2003, **175**, 373–392.

Chu, J-Z., Shieh, S-S., Jang, S-S., Chien, C-I., Wan, H-P. and Ko, H-H., Constrained optimization of combustion in a simulated coal-fired boiler using artificial neural network model and information analysis. *Fuel*, 2003, **82**, 693–703.

Cohon, J.L., *Multiobjective Programming and Planning*, 1978 (Academic Press: New York).

Das, I. and Dennis, J.E., A closer look at drawbacks of minimizing weighted sums of objectives for Pareto set generation in multicriteria optimization problems. *Structural and Multidisciplinary Optimization*, 1997, **14**, 63–69.

Deb, K., *Multi-Objective Optimization Using Genetic Algorithms*, 2001 (John Wiley & Sons: Chichester).

Duo, W., Dam-Johansen, K. and Østergaard, K., Kinetics of the gas-phase reaction between nitric oxide, ammonia and oxygen. *Canadian Journal of Chemical Engineering*, 1992, **70**, 1014–1020.

Elliot, L., Ingham, D.B., Kyne, A.G., Mera, N.S., Pourkashanian, M. and Wilson, C.W., Genetic algorithms for optimisation of chemical kinetics reaction mechanisms. *Progress in Energy and Combustion Science*, 2004, **30**, 297–328.

Ertesvåg, I.S. and Magnussen, B.F., The eddy dissipation turbulence energy cascade model. *Combustion Science and Technology*, 2000, **159**, 213–235.

Fluent Inc., *Fluent 6.2. User's Guide*, 2005, http://www.fluent.com.

Fonseca, C.M. and Fleming, P.J., Multiobjective optimization, In: T. Bäck, D.B. Fogel and Z. Michalewicz, eds. *Evolutionary Computation 2 – Advanced*

*Algorithms and Operators*, 2000 (Institute of Physics Publishing: Bristol), 25–37.

Giannakoglou, K.C., Design of optimal aerodynamic shapes using stochastic optimization methods and computational intelligence. *Progress in Aerospace Sciences*, 2001, **38**, 43–76.

Giannakoglou, K.C. and Giotis, A.P., *The Evolutionary Algorithm System EASY version 1.5*, 2007, National Technical University of Athens, Greece, http://147.102.55.162/EASY/.

Hämäläinen, J.P., Malkamäki, T. and Toivanen, J., Genetic algorithms in shape optimization of a paper machine headbox, In: K. Miettinen, M.M. Mäkelä, P. Neittaanmäki and J. Périaux, eds. *Evolutionary Algorithms in Engineering and Computer Science*, 1999 (John Wiley & Sons: Chichester), 435–443.

Homma, R. and Chen, J-Y., Combustion process optimization by genetic algorithms: reduction of $NO_2$ emission via optimal postflame process. *Proceedings of the Combustion Institute*, 2000, **28**, 2483–2489.

Johnson, R.W., Landon, M.D. and Perry, E.C., Design optimization, In: C.E. Baukal, V.Y. Gershtein and X. Li, eds. *Computational Fluid Dynamics in Industrial Combustion*, 2001 (CRC Press: Boca Raton), 557–584.

Jones, W.P. and Lindstedt, R.P. *Combustion and Flame*, 1988, **73**, 233–249.

Kalogirou, S.A., Artificial intelligence for the modeling and control of combustion processes: a review. *Progress in Energy and Combustion Science*, 2003, **29**, 515–566.

Koski, J., Defectiveness of weighting method in multicriterion optimization of structures. *Communications in Applied Numerical Methods*, 1985, **1**, 333–337.

Magnussen, B.F. and Hjertager B.H., On mathematical modeling of turbulent combustion with special emphasis on soot formation and combustion. *Proceedings of the Combustion Institute*, 1976, **16**, 719–729.

Marler, R.T. and Arora, J.S., Survey of multi-objective optimization methods for engineering. *Structural and Multidisciplinary Optimization*, 2004, **26**, 369–395.

Miettinen, K., *Nonlinear Multiobjective Optimization*, 1999 (Kluwer Academic Publishers: Boston).

Miller, J.A. and Bowman, C.T., Mechanism and modeling of nitrogen chemistry in combustion. *Progress in Energy and Combustion Science*, 1989, **15**, 287–338.

Montgomery, C.J., Yang, C., Parkinson, A.R. and Chen, J-Y., Selecting the optimum quasi-steady-state species for reduced chemical kinetic mechanisms using a genetic algorithm. *Combustion and Flame*, 2006, **144**, 37–52.

Osyczka, A., *Evolutionary Algorithms for Single and Multicriteria Design Optimization*, 2002 (Physica-Verlag: Heidelberg).

Poinsot, T. and Veynante, D., *Theoretical and Numerical Combustion* (2nd edn), 2005 (R.T. Edwards: Philadelphia).

Polifke, W., Geng, W. and Döbbeling, K., Optimization of rate constants for simplified reaction mechanisms with genetic algorithms. *Combustion and Flame*, 1998, **113**, 119–135.

Poloni, C., Giurgevich, A., Onesti, L. and Pediroda, V., Hybridization of a multi-objective genetic algorithm, a neural network and a classical optimizer for a complex design problem in fluid dynamics. *Computer Methods in Applied Mechanics and Engineering*, 2000, **186**, 403–420.

Radojevic, M., Reduction of nitrogen oxides in flue gases. *Environmental Pollution*, 1998, **102, S1**, 685–689.

Raithby, G.D. and Chui, E.H., A finite-volume method for predicting a radiant heat transfer in enclosures with participating media. *Journal of Heat Transfer–Transactions of the ASME*, 1990, **112**, 415–423.

Risio, B., Blum, F., Hetzer, J., Berreth, A., Schnell, U. and Hein, K.R.G., Towards an innovative virtual optimisation machine for the power industry. *Progress in Computational Fluid Dynamics*, 2005, **5**, 398–405.

Saario, A. and Oksanen, A., Comparison of global ammonia chemistry mechanisms in biomass combustion and selective noncatalytic reduction process conditions. *Energy & Fuels*, 2008a, **22**, 297–305.

Saario, A. and Oksanen, A., Effect of computational grid in industrial-scale boiler modeling. *International Journal of Numerical Methods for Heat & Fluid Flow*, 2008b, accepted for publication.

Saario, A., Oksanen, A. and Ylitalo, M., Combination of genetic algorithm and computational fluid dynamics in combustion process emission minimisation. *Combustion Theory and Modelling*, 2006, **10**, 1037–1047.

Shih, T-H., Liou, W.W., Shabbir, A., Yang, Z. and Zhu, J., A new $k$-$\varepsilon$ eddy viscosity model for high Reynolds number turbulent flows. *Computers & Fluids*, 1995, **24**, 227–238.

Smith, T.F., Shen, Z.F. and Friedman, J.N., Evaluation of coefficients for the weighted sum of gray gases model. *Journal of Heat Transfer–Transactions of the ASME*, 1982, **104**, 602–608.

Tan, C.K., Wilcox, S.J. and Ward, J., Use of artificial intelligence techniques for optimisation of co-combustion of coal with biomass. *Journal of the Institute of Energy*, 2006, **79**, 19–25.

Ward, J., Tan, C-K., Chong, A. and Wilcox, S., The application of artificial intelligence in combustion engineering. In: *7th European Conference on Industrial Furnaces and Boilers*, Oporto, Portugal, 2006, April 18–21.

Wierzbicki, A.P., A mathematical basis for satisficing decision making. *Mathematical Modelling*, 1982, **3**, 391–405.

Zhou, H., Cen, K. and Fan, J., Multi-objective optimization of the coal combustion performance with artificial neural networks and genetic algorithms. *International Journal of Energy Research*, 2005, **29**, 499–510.

Zhou, H., Cen, K. and Mao, J., Combining neural network and genetic algorithms to optimize low $NO_x$ pulverized coal combustion. *Fuel*, 2001, **80**, 2163–2169.

# Figure captions

Figure 1. Boiler sketch.

Figure 2. Location and numbering of $NH_3$ injections at height of 7.5 m (contours correspond to $NH_3$ concentration ($ppm_{vol}$)). View from boiler roof.

Figure 3. Ideal and nadir objective vectors. Symbol $Z$ is image of feasible set $S$ in objective space.

Figure 4. Principle of genetic algorithm. Particular details related to present study are indicated in square brackets.

Figure 5. Principle of Powell's conjugate direction method. Particular details related to present study are indicated in square brackets.

Figure 6. Predicted current operating point ("Current design"), four predicted solutions from Pareto optimal set, and two reference points in objective space.

Figure 7. Predicted Pareto optimal solutions in design space. The dashed line indicates injection settings of current operating point. Design variables $i \in \{1, 2, \ldots, 9\}$ are denoted by $i \in \{$Rear, Front left, Side left A, Side left B, Side left C, Front right, Side right A, Side right B, Side right C$\}$, respectively.

Figure 7(a). Minimize only NO emission ("SOO NO" in figure 6). Solid line indicates upper design variable bounds. $f_1(\boldsymbol{x}) = 53.1\ \mathrm{ppm_{vol}}$, $f_2(\boldsymbol{x}) = 47.5\ \mathrm{ppm_{vol}}$, and $g(\boldsymbol{x}) = 0.0005\ \mathrm{kg_{NH_3}\ s^{-1}}$ (violated).

Figure 7(b). Minimize both NO and $NH_3$ emission ("MOO I" in figure 6). $f_1(\boldsymbol{x}) = 66.8\ \mathrm{ppm_{vol}}$, $f_2(\boldsymbol{x}) = 11.8\ \mathrm{ppm_{vol}}$, and $g(\boldsymbol{x}) = -0.0021\ \mathrm{kg_{NH_3}\ s^{-1}}$ (inactive).

Figure 7(c). Minimize both NO and $NH_3$ emission ("MOO II" in figure 6). $f_1(\boldsymbol{x}) = 61.9\ \mathrm{ppm_{vol}}$, $f_2(\boldsymbol{x}) = 19.7\ \mathrm{ppm_{vol}}$, and $g(\boldsymbol{x}) = -0.0008\ \mathrm{kg_{NH_3}\ s^{-1}}$ (inactive).

Figure 8. Predicted points in objective space. All feasible points and points which exceed $\dot{m}_{\mathrm{NH_3,max}}$ at maximum by 5% are shown.

Figure 9. Enlargement of Pareto set in objective space. All predicted points which exceed $\dot{m}_{\mathrm{NH_3,max}}$ at maximum by 5% are shown. The final solution is selected from among four solutions indicated by white markers. The selection criterion of DMs is based on the guaranteed emission limit of $NH_3$ ($f_{2,\mathrm{guar}}(\boldsymbol{x}) = 15\ \mathrm{ppm_{vol}}$).

Figure 10. Predicted optional good solutions in design space. The dashed line indicates injection settings of current operating point. The limiting objective, i.e. the objective which has a greater normalized distance to the reference point according to the achievement function (see first term in equation (10)), is marked with an asterisk *.

Figure 10(a). Optional solution "a" in figure 9. Found with "Reference point I". $f_1(\boldsymbol{x}) = 64.0$ $\text{ppm}_{\text{vol}}$, $^*f_2(\boldsymbol{x}) = 14.3$ $\text{ppm}_{\text{vol}}$ and $g(\boldsymbol{x}) = -0.0017$ $\text{kg}_{\text{NH}_3}$ $\text{s}^{-1}$ (inactive).

Figure 10(b). Optional solution "b" in figure 9. Found with "Reference point II". $^*f_1(\boldsymbol{x}) = 64.9$ $\text{ppm}_{\text{vol}}$, $f_2(\boldsymbol{x}) = 12.7$ $\text{ppm}_{\text{vol}}$ and $g(\boldsymbol{x}) = -0.0018$ $\text{kg}_{\text{NH}_3}$ $\text{s}^{-1}$ (inactive).

Figure 10(c). Optional solution "c" in figure 9. Found with "Reference point I". $f_1(\boldsymbol{x}) = 66.0$ $\text{ppm}_{\text{vol}}$, $^*f_2(\boldsymbol{x}) = 11.9$ $\text{ppm}_{\text{vol}}$ and $g(\boldsymbol{x}) = -0.0030$ $\text{kg}_{\text{NH}_3}$ $\text{s}^{-1}$ (inactive).

Figure 10(d). Final solution in figure 9. Found with "Reference point II". $^*f_1(\boldsymbol{x}) = 66.8$ $\text{ppm}_{\text{vol}}$, $f_2(\boldsymbol{x}) = 10.9$ $\text{ppm}_{\text{vol}}$ and $g(\boldsymbol{x}) = -0.0003$ $\text{kg}_{\text{NH}_3}$ $\text{s}^{-1}$ (inactive).

Figure 11. Robustness of final solution. Injection "Side right C", $X_9$, is varied from the lower to the upper bound. The achievement function method applied aims at reducing the NO emission when $X_9 < 0.21$ vol-%, otherwise it aims at reducing the $NH_3$ emission (see also equation (10)). Constraint $g(\boldsymbol{x})$ is violated when $X_9 \geq 3.14$ vol-%.

Figure 12. CFD predictions of current operating point at height of 7.5 m.

Figure 12(a). Contours of temperature (K)

Figure 12(b). Contours of CO (vol-%)

Figure 12(c). Contours of $O_2$ (vol-%)

Figure 12(d). Contours of NO ($\text{ppm}_{\text{vol}}$)

Figure 12(e). Contours of $NH_3$ ($\text{ppm}_{\text{vol}}$)

Figure 12(f). Contours of vertical velocity $u_z$ ($\text{m s}^{-1}$)

Figure 13. Three experimental points, CFD predictions corresponding to three experimental points and four points obtained from Pareto set in objective space. "100% injection" corresponds to current operating point and "exp." denotes experimental.

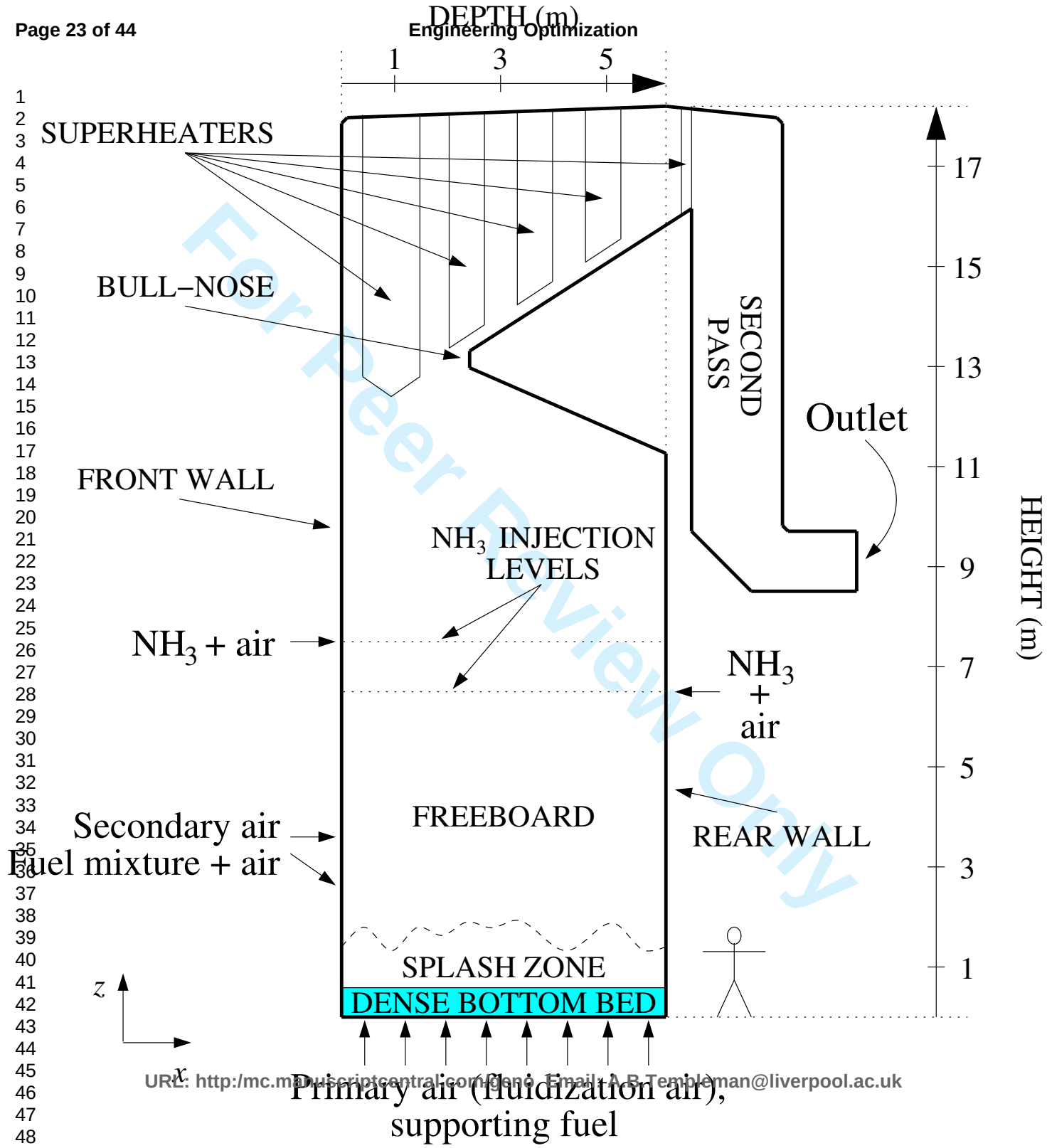

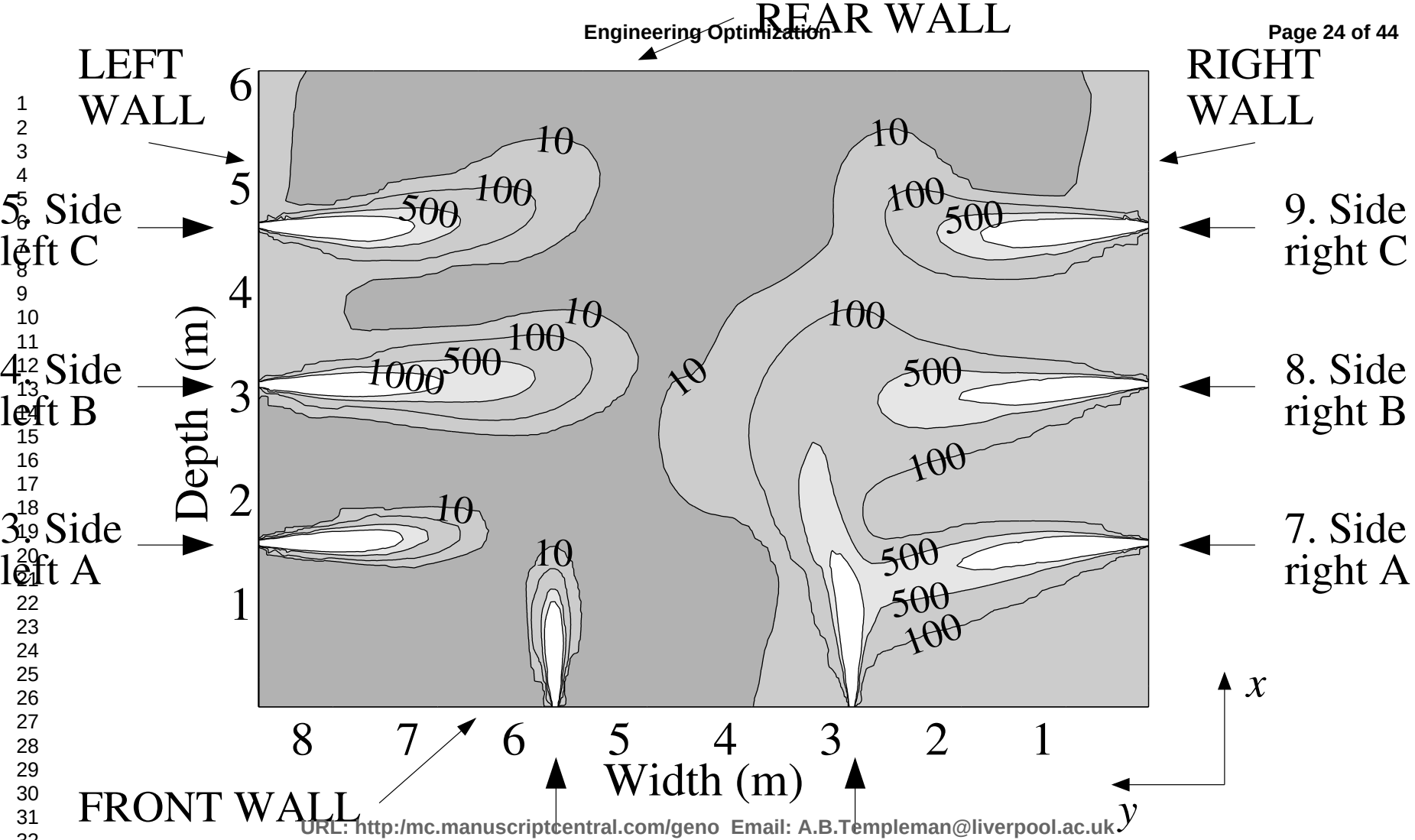
REAR WALL
LEFT WALL
RIGHT WALL
5. Side left C
4. Side left B
3. Side left A
9. Side right C
8. Side right B
7. Side right A
Depth (m)
6
5
4
3
2
1
10
100
500
1000
8 7 6 5 4 3 2 1
Width (m)
FRONT WALL
x
y
2. Front left
6. Front right

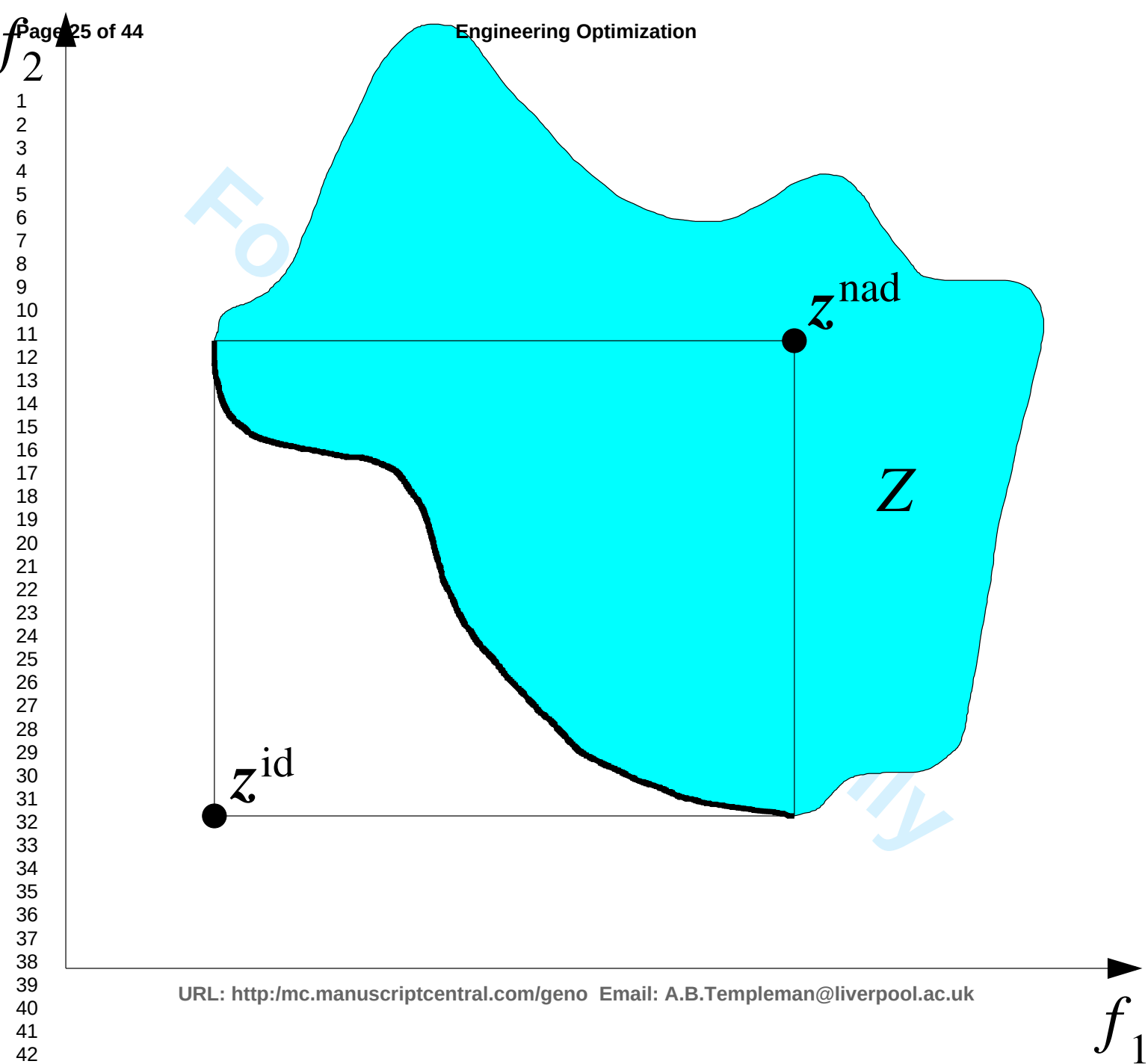
$f_2$
$z^{nad}$
$z$
$z^{id}$
$f_1$

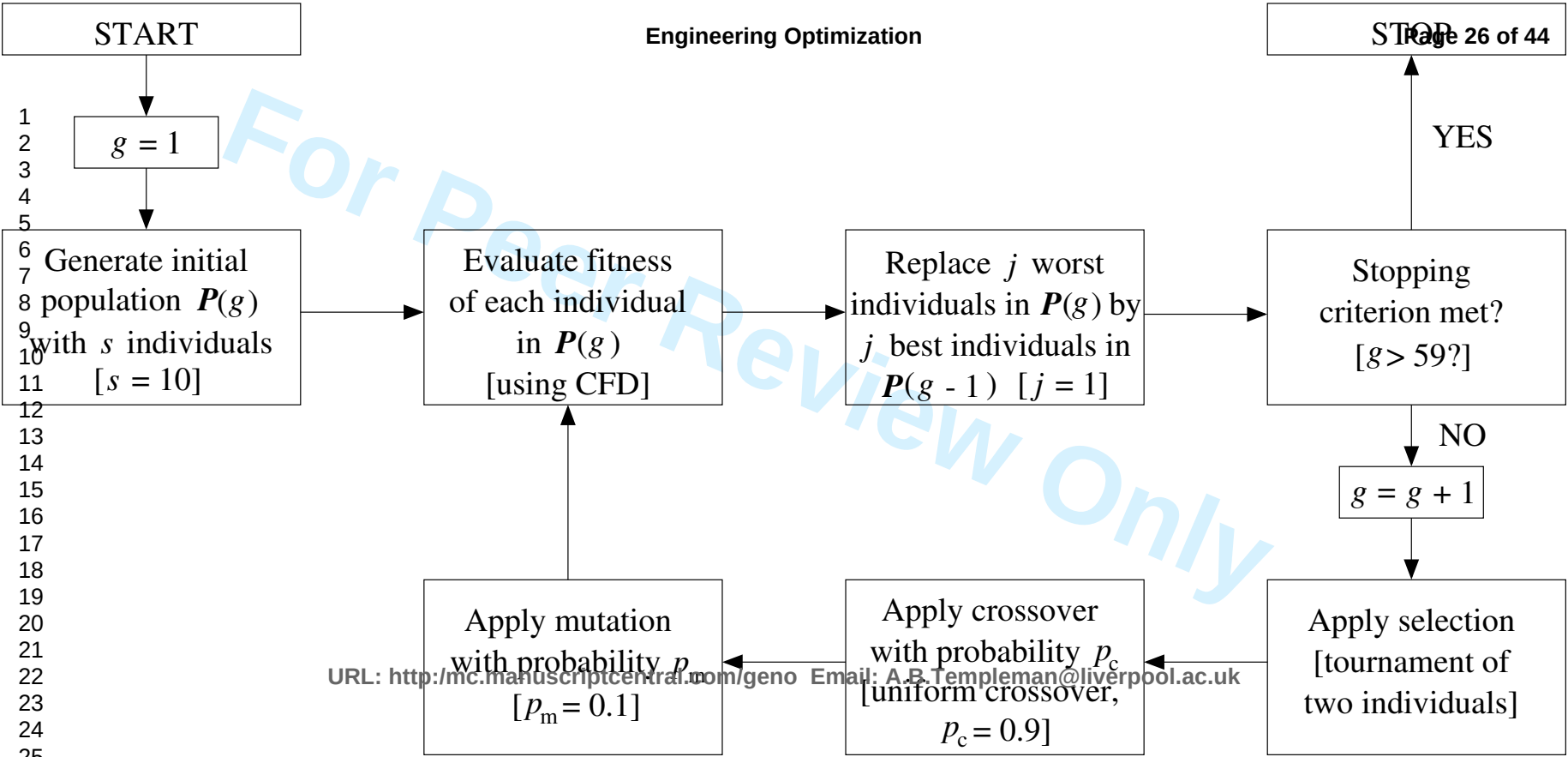

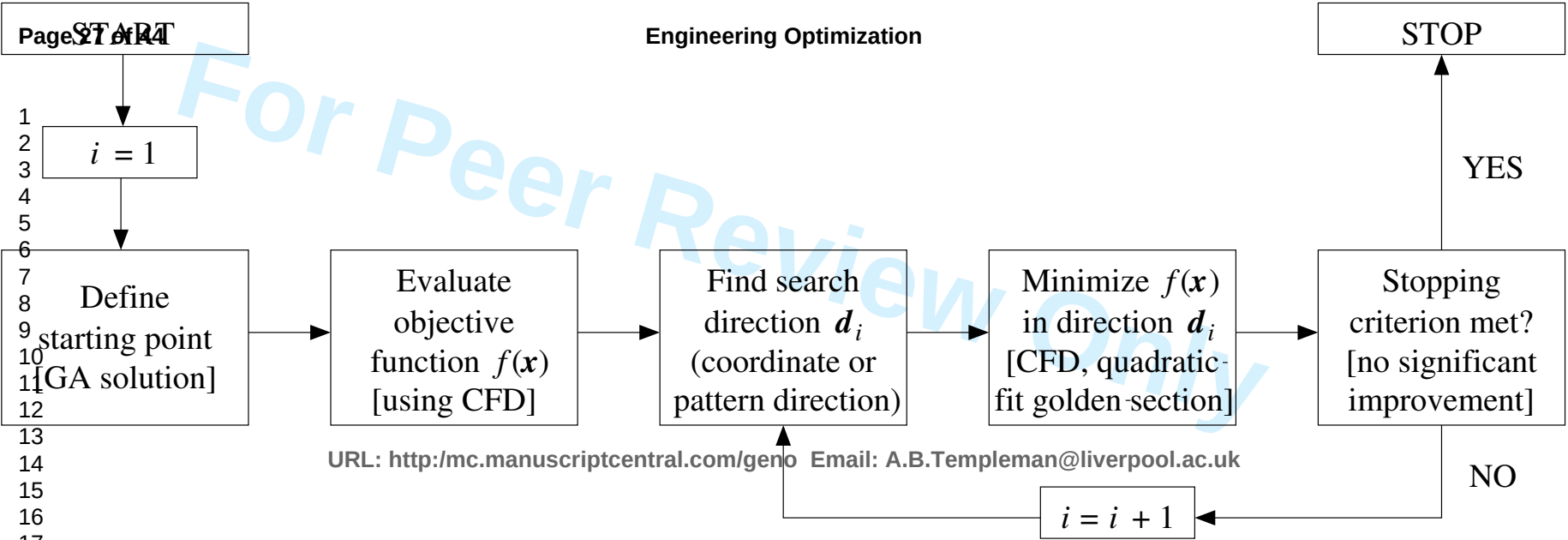

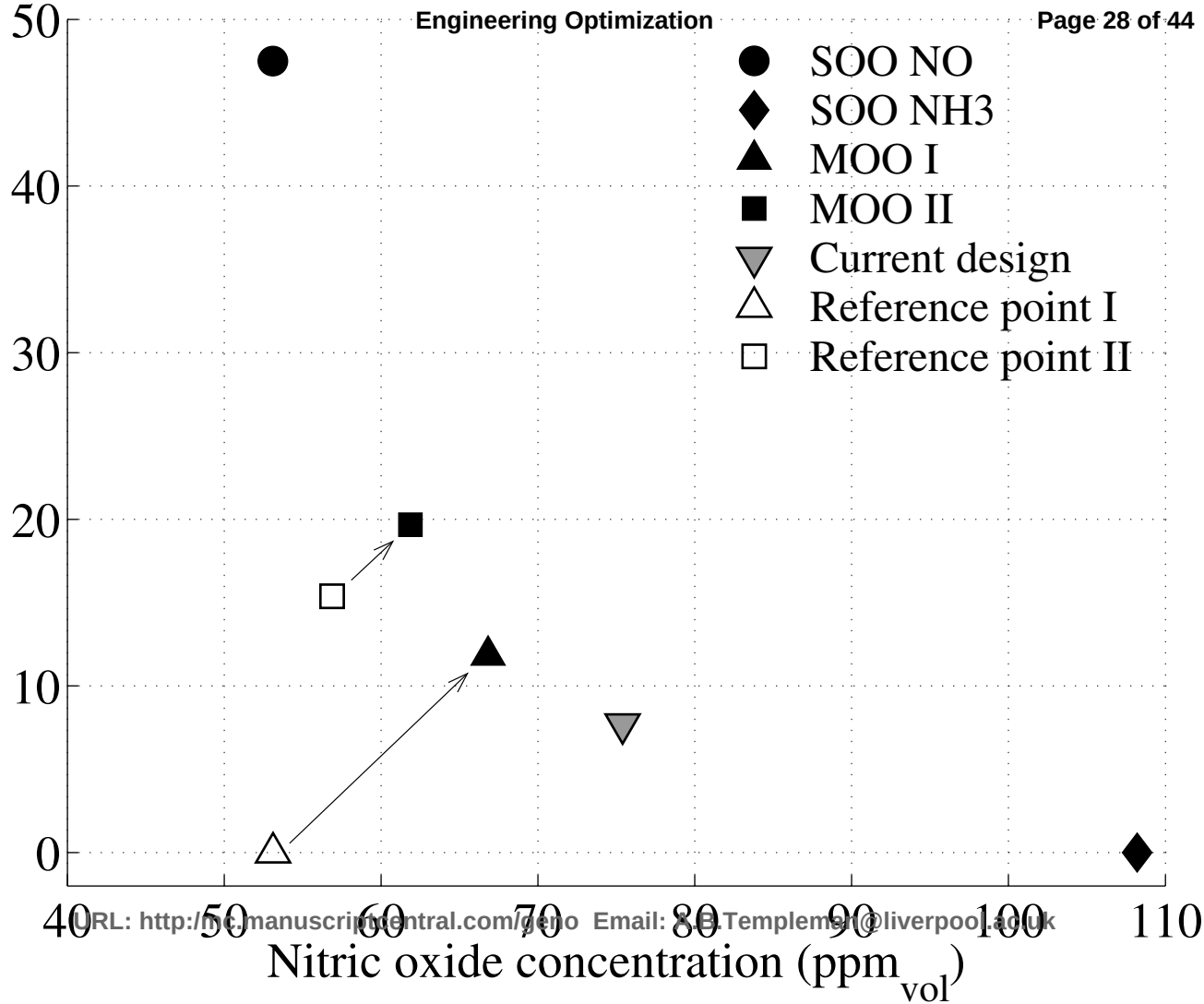
SOO NO
SOO NH3
MOO I
MOO II
Current design
Reference point I
Reference point II
Ammonia concentration (ppm vol)
Nitric oxide concentration (ppm vol)
0
10
20
30
40
50
40
50
60
70
80
90
100
110

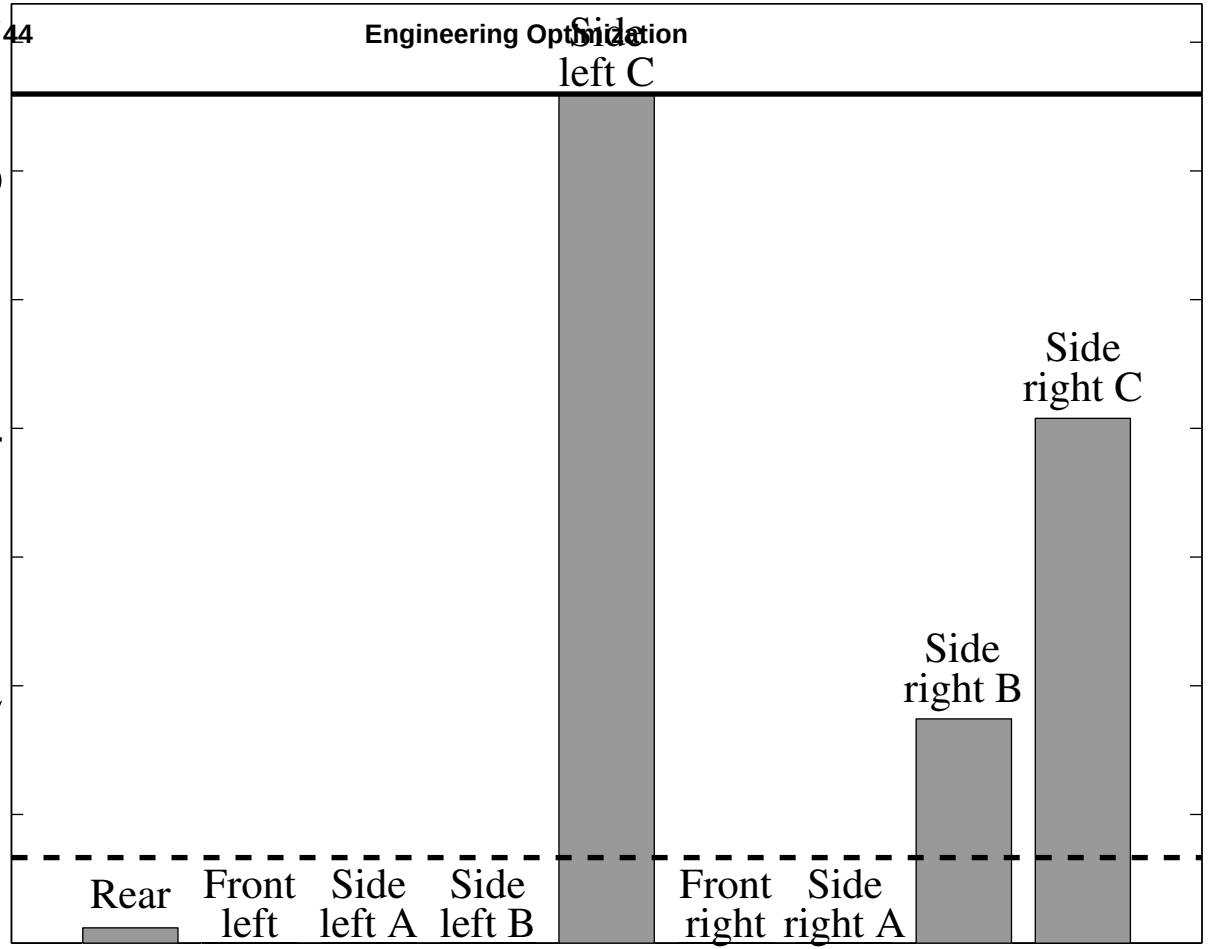


$NH_3$ concentration (vol−%)



Injection

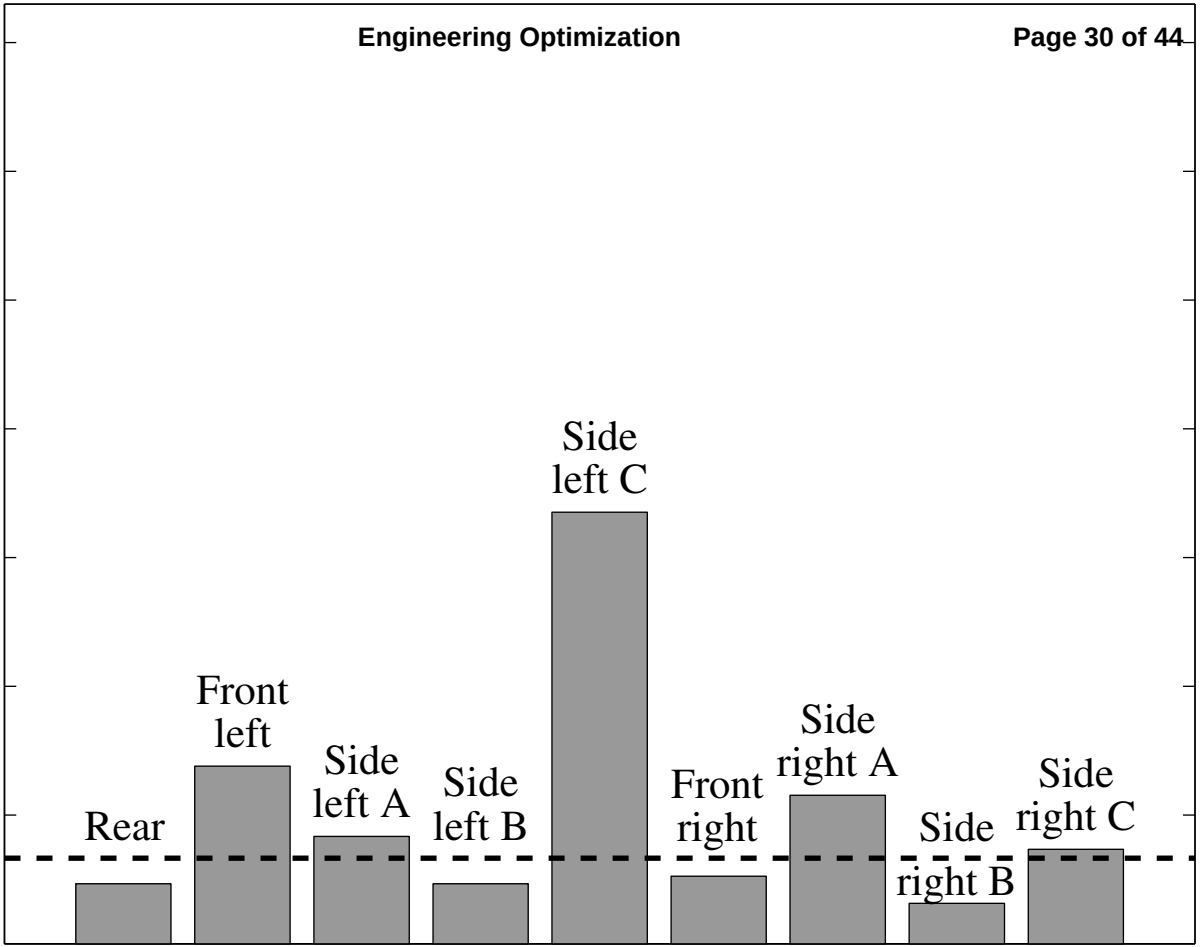
7
6
5
4
3
2
1
Rear
Front left
Side left A
Side left B
Side left C
Front right
Side right A
Side right B
Side right C
$NH_3$ concentration (vol−%)
Injection

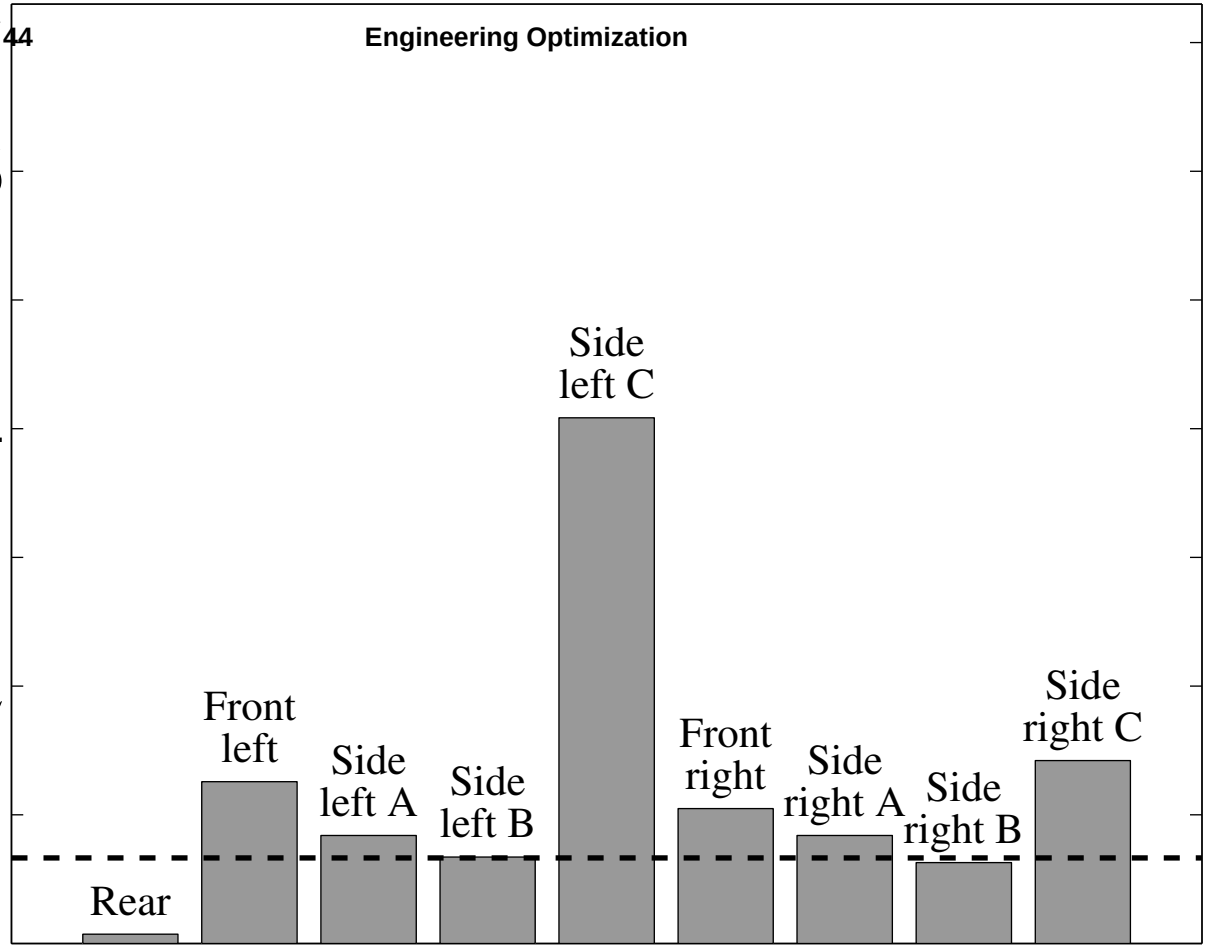
7
6
5
4
3
2
1
$NH_3$ concentration (vol−%)
Rear
Front left
Side left A
Side left B
Side left C
Front right
Side right A
Side right B
Side right C
Injection

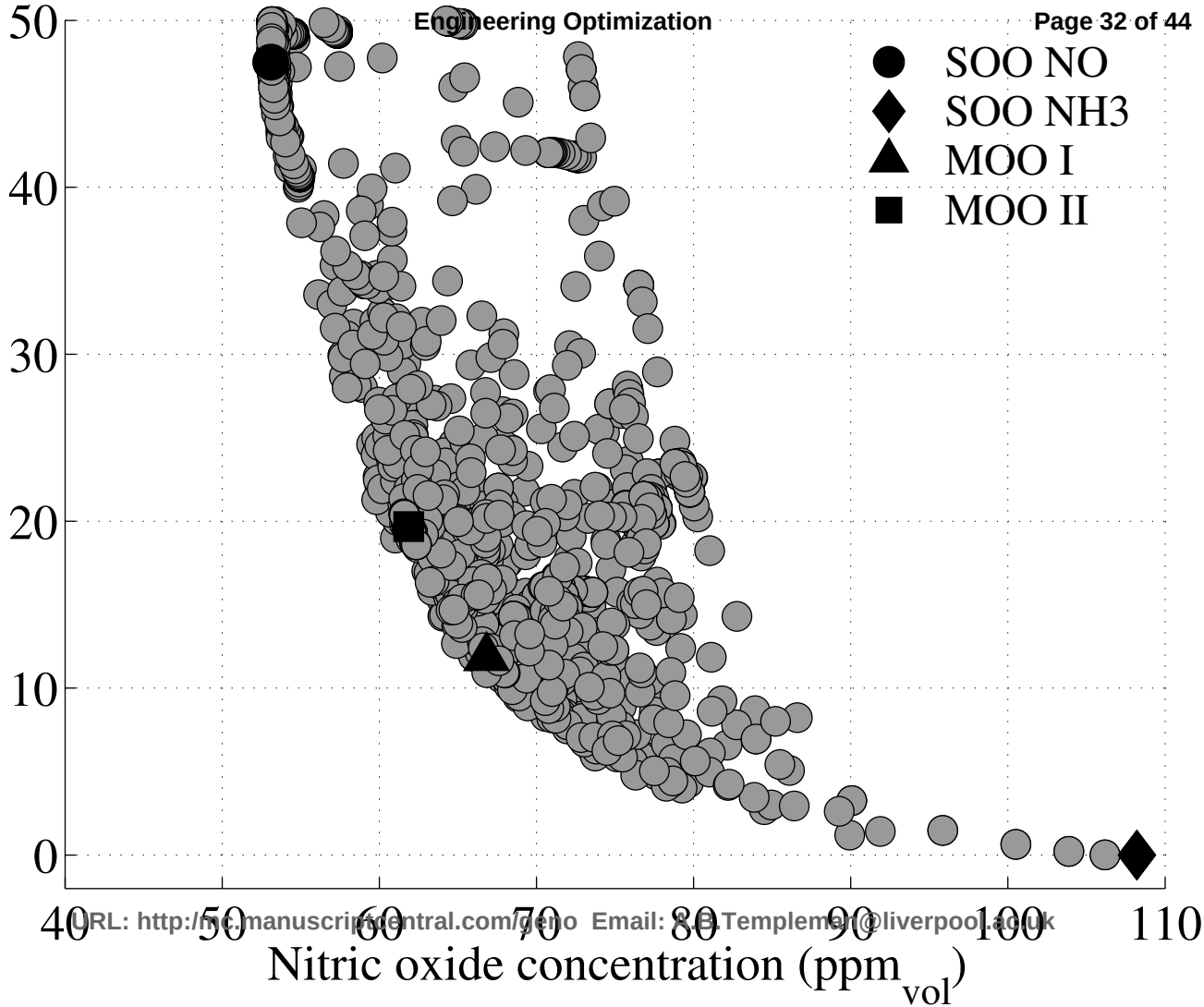
SOO NO
SOO NH3
MOO I
MOO II
Ammonia concentration (ppm vol)
Nitric oxide concentration (ppm vol)
0
10
20
30
40
50
40
50
60
70
80
90
100
110

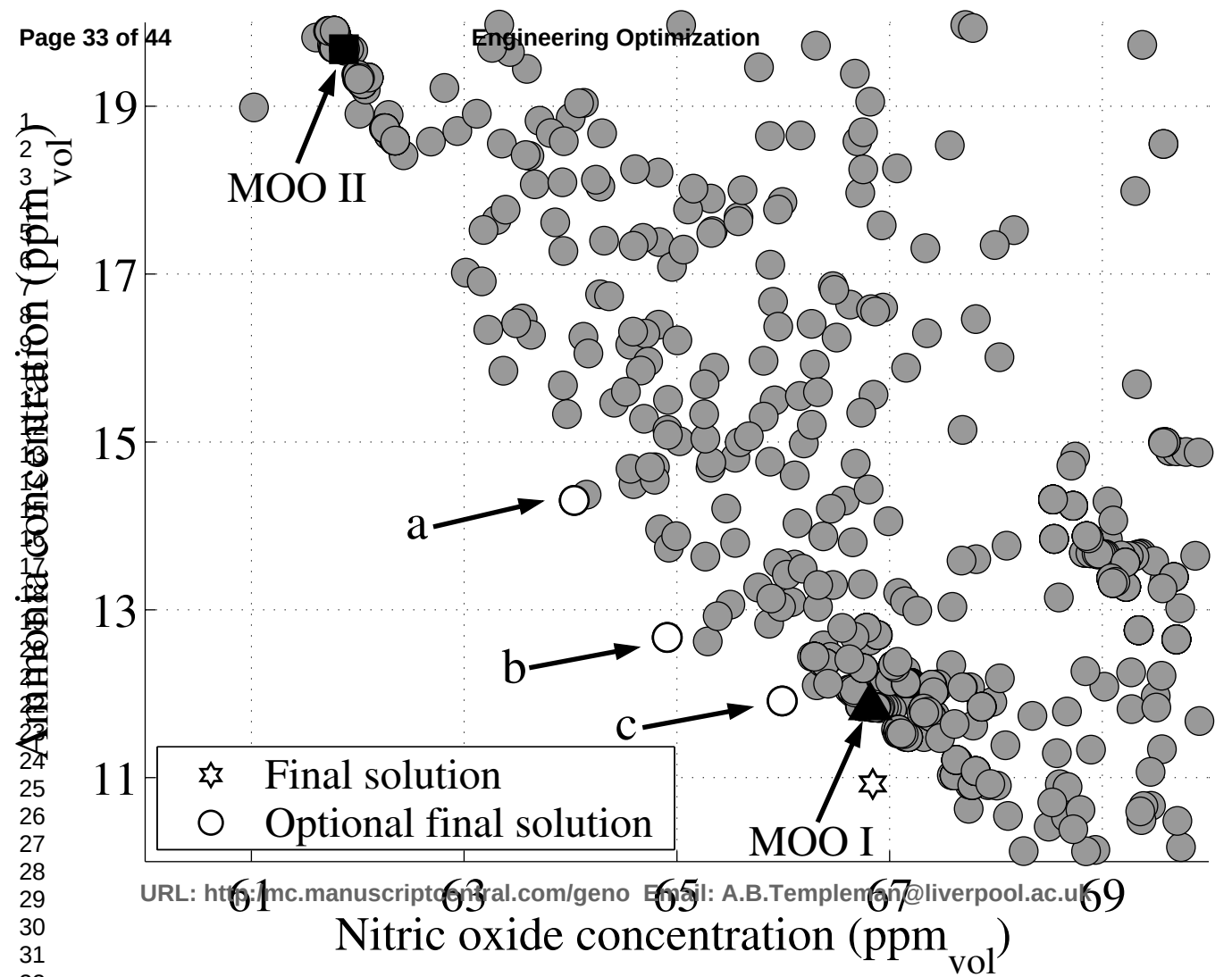
MOO II
a
b
c
MOO I
Final solution
Optional final solution
19
17
15
13
11
61
63
65
67
69
Nitric oxide concentration (ppm vol)
Ammonia concentration (ppm vol)

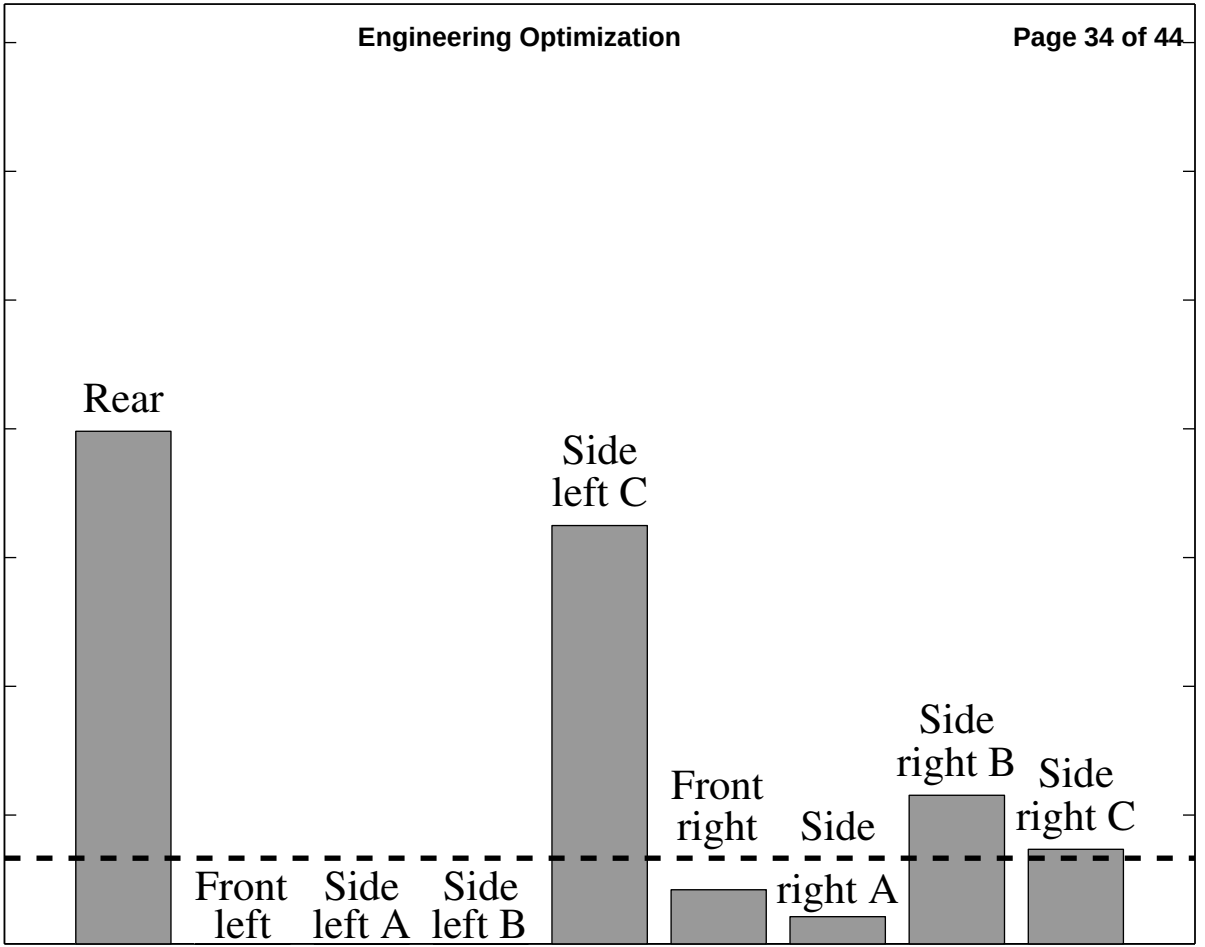
7
6
5
4
3
2
1
Rear
Front left
Side left A
Side left B
Side left C
Front right
Side right A
Side right B
Side right C
NH3 concentration (vol−%)
Injection

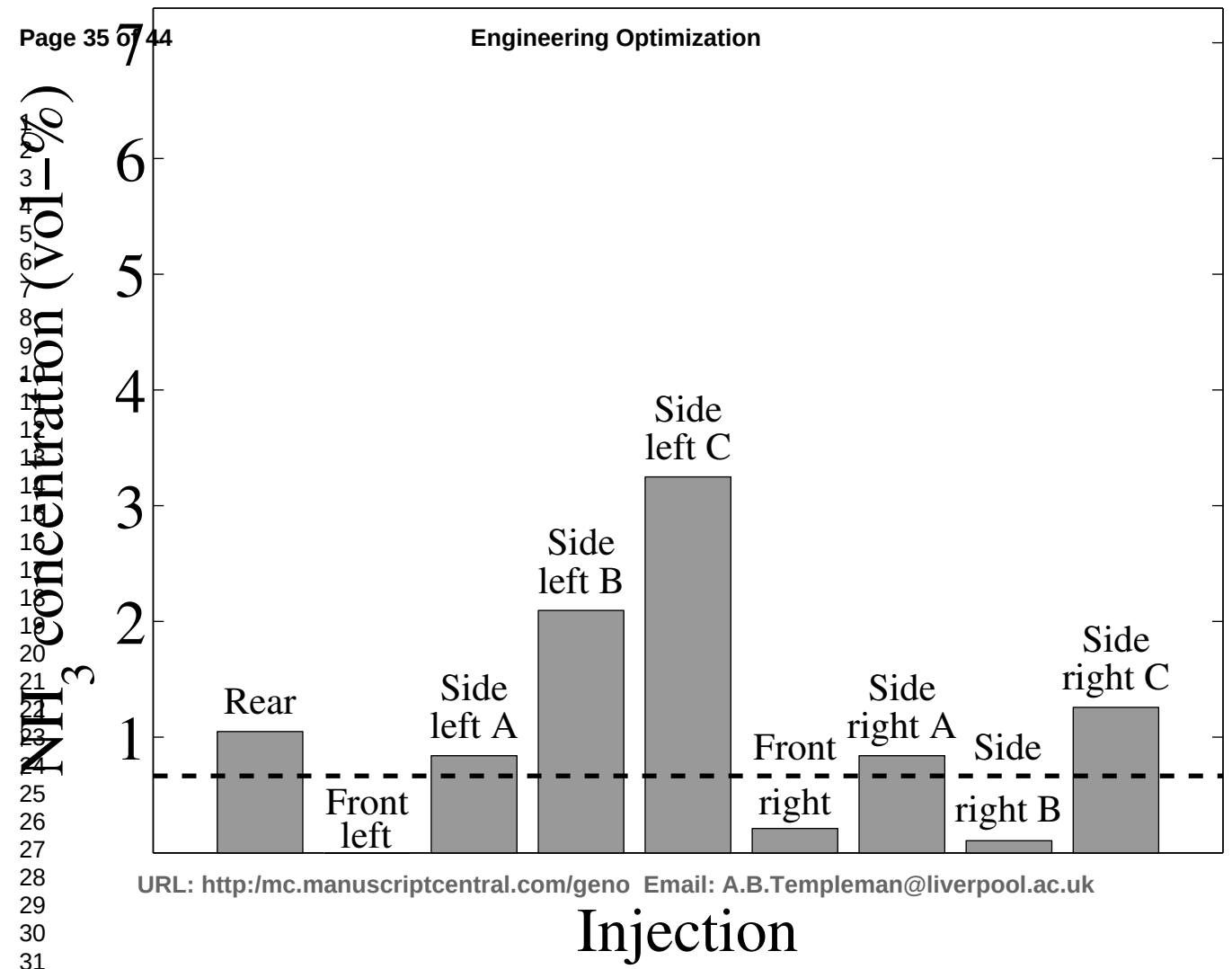
NH3 concentration (vol−%)
7
6
5
4
3
2
1
Rear
Front left
Side left A
Side left B
Side left C
Front right
Side right A
Side right B
Side right C
Injection

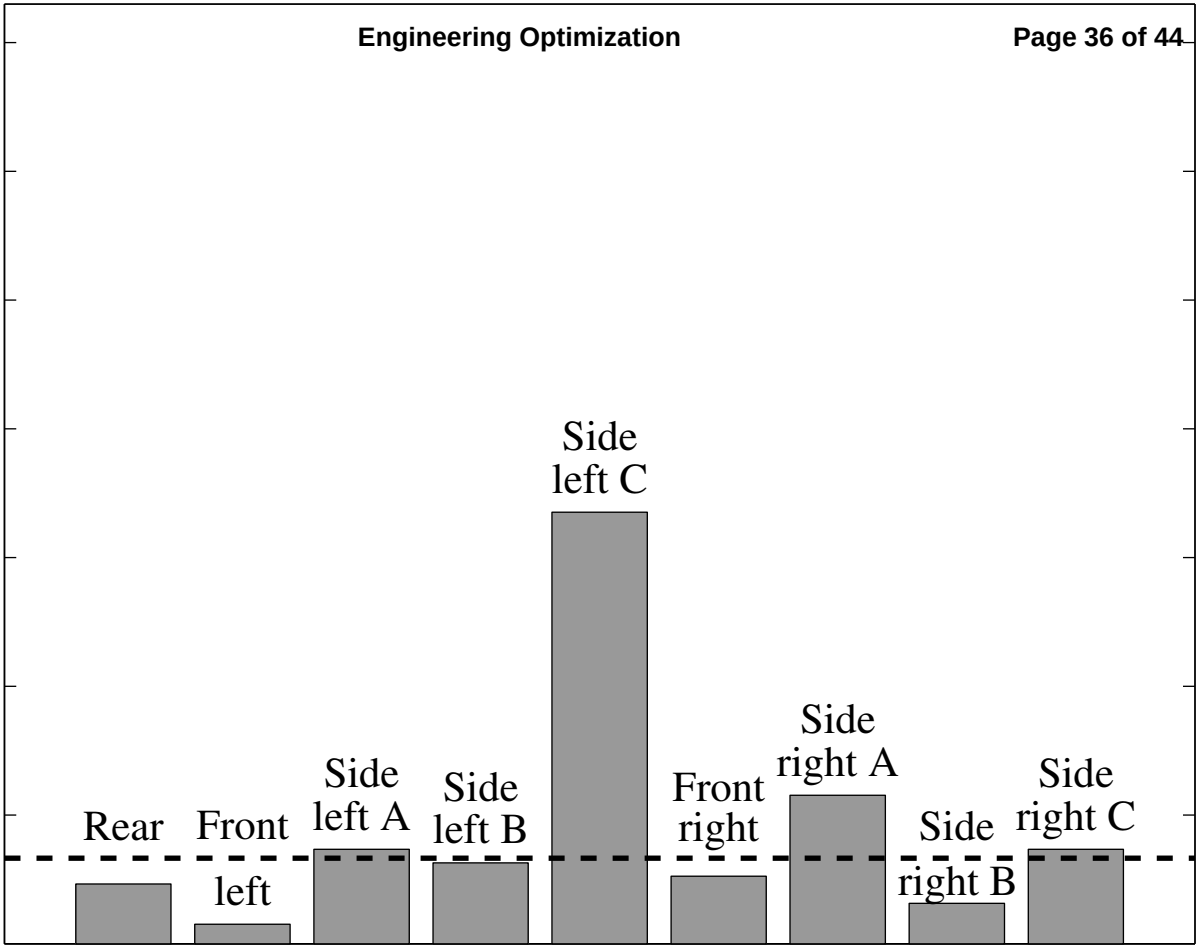
7
6
5
4
3
2
1
$NH_3$ concentration (vol−%)
Rear
Front left
Side left A
Side left B
Side left C
Front right
Side right A
Side right B
Side right C
Injection

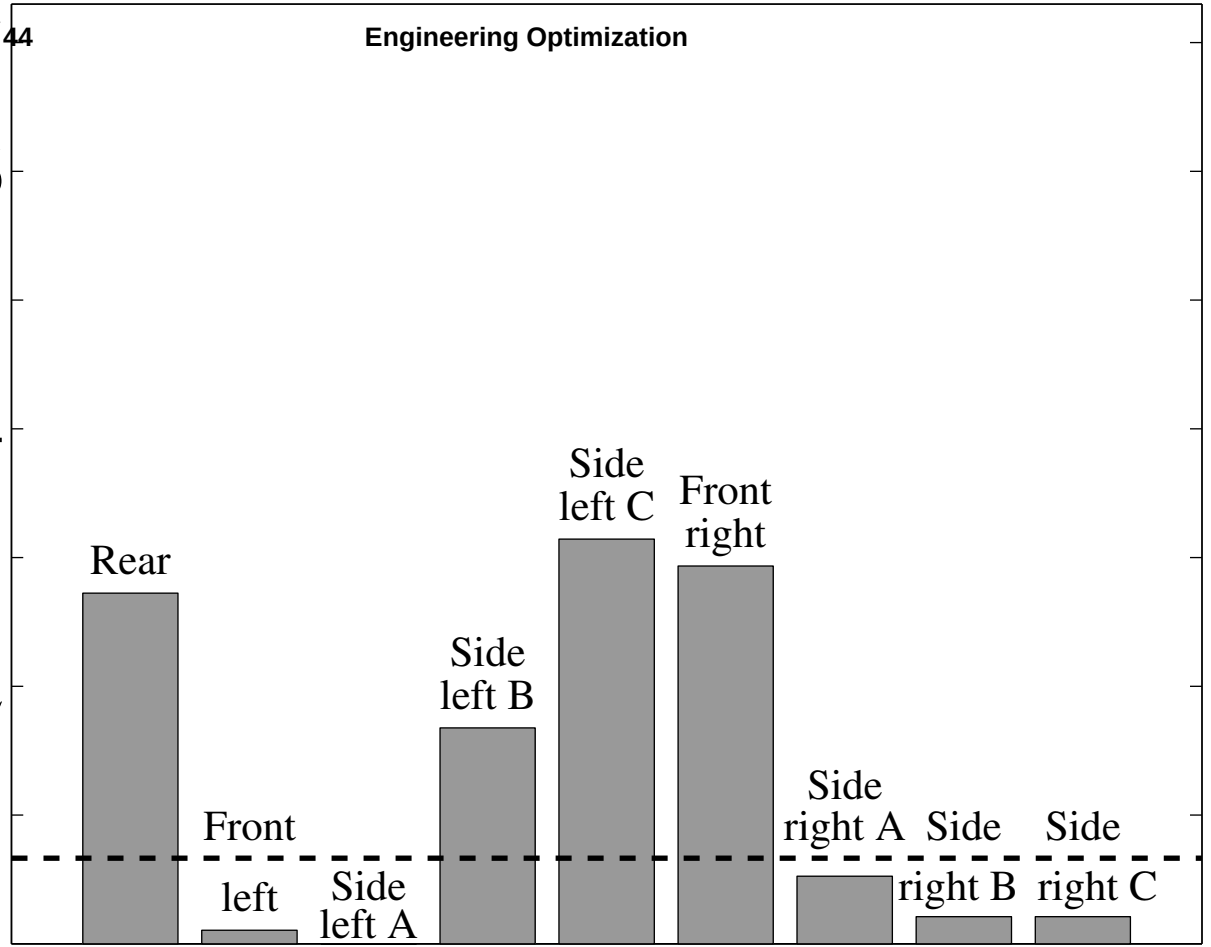
7
6
5
4
3
2
1
$NH_3$ concentration (vol−%)
Rear
Front left
Side left A
Side left B
Side left C
Front right
Side right A
Side right B
Side right C
Injection

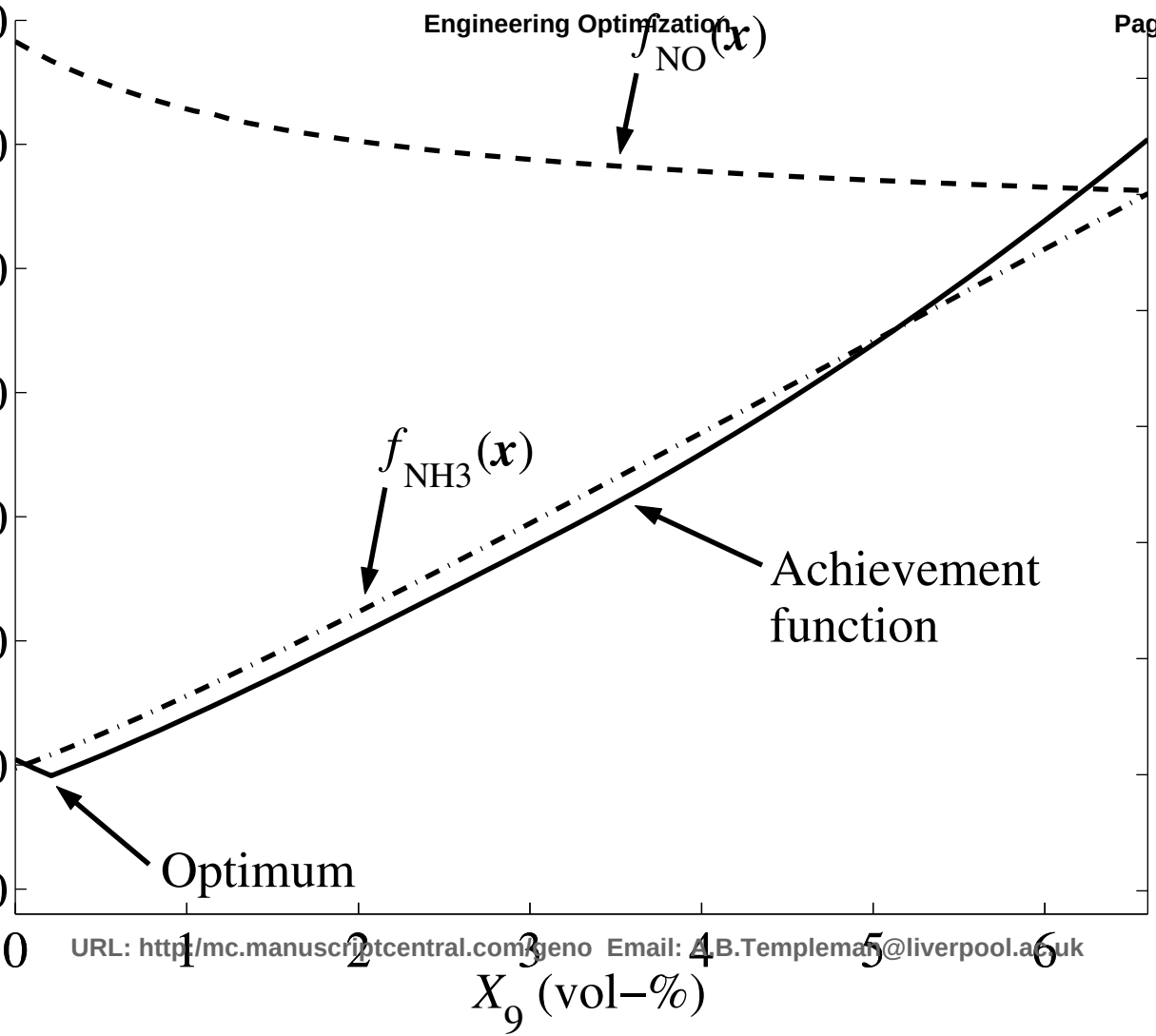
$f_{NO}(x)$
$f_{NO}(x)$ and $f_{NH3}(x)$ (ppm$_{vol}$)
$f_{NH3}(x)$
Achievement function
Optimum
$X_9$ (vol–%)
Achievement function value
70
60
50
40
30
20
10
0
1.2
1.0
0.8
0.6
0.4
0.2
0.0
–0.2
0
1
2
3
4
5
6

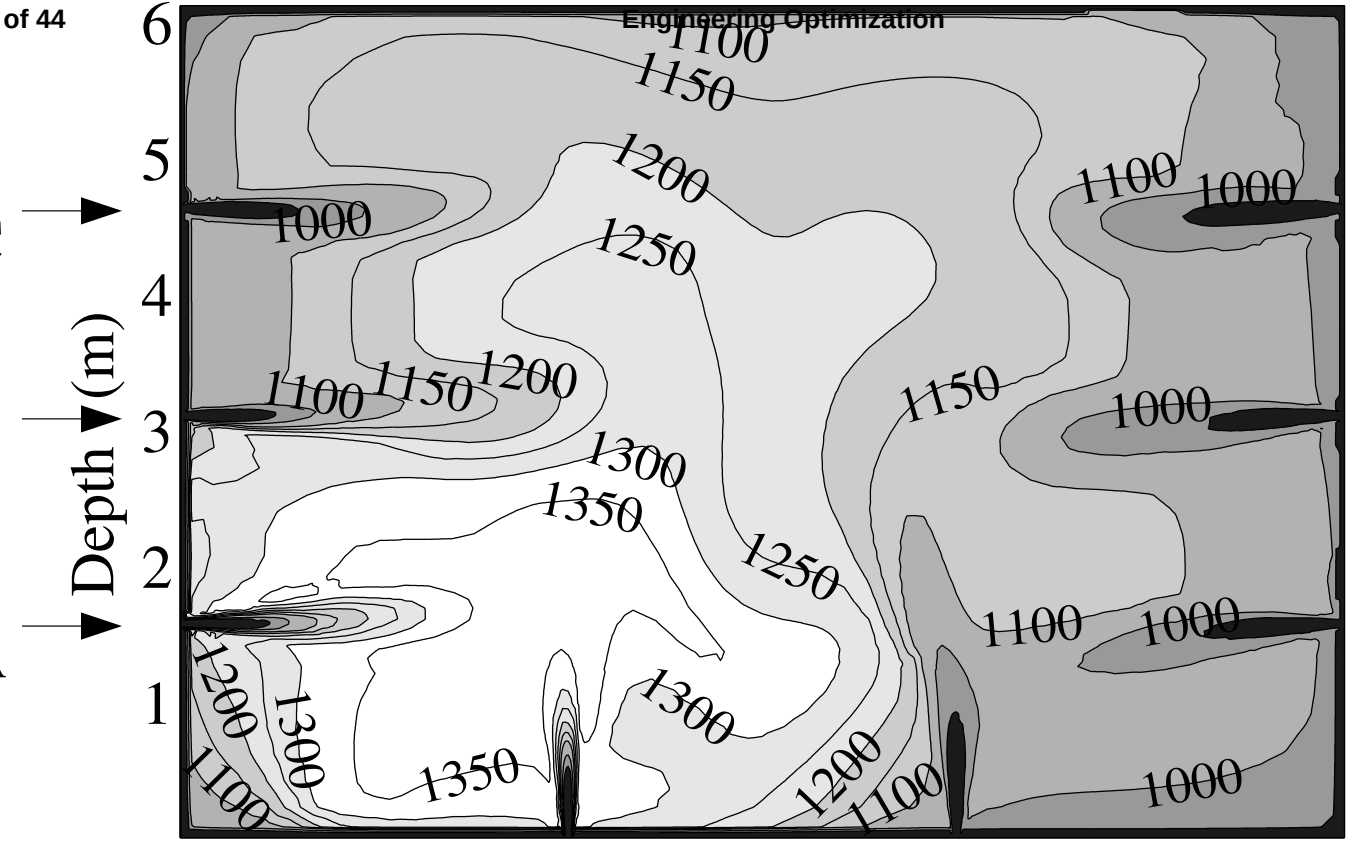


Side left C

Side left B

Side left A

Side right C

Side right B

Side right A

Front left

Front right

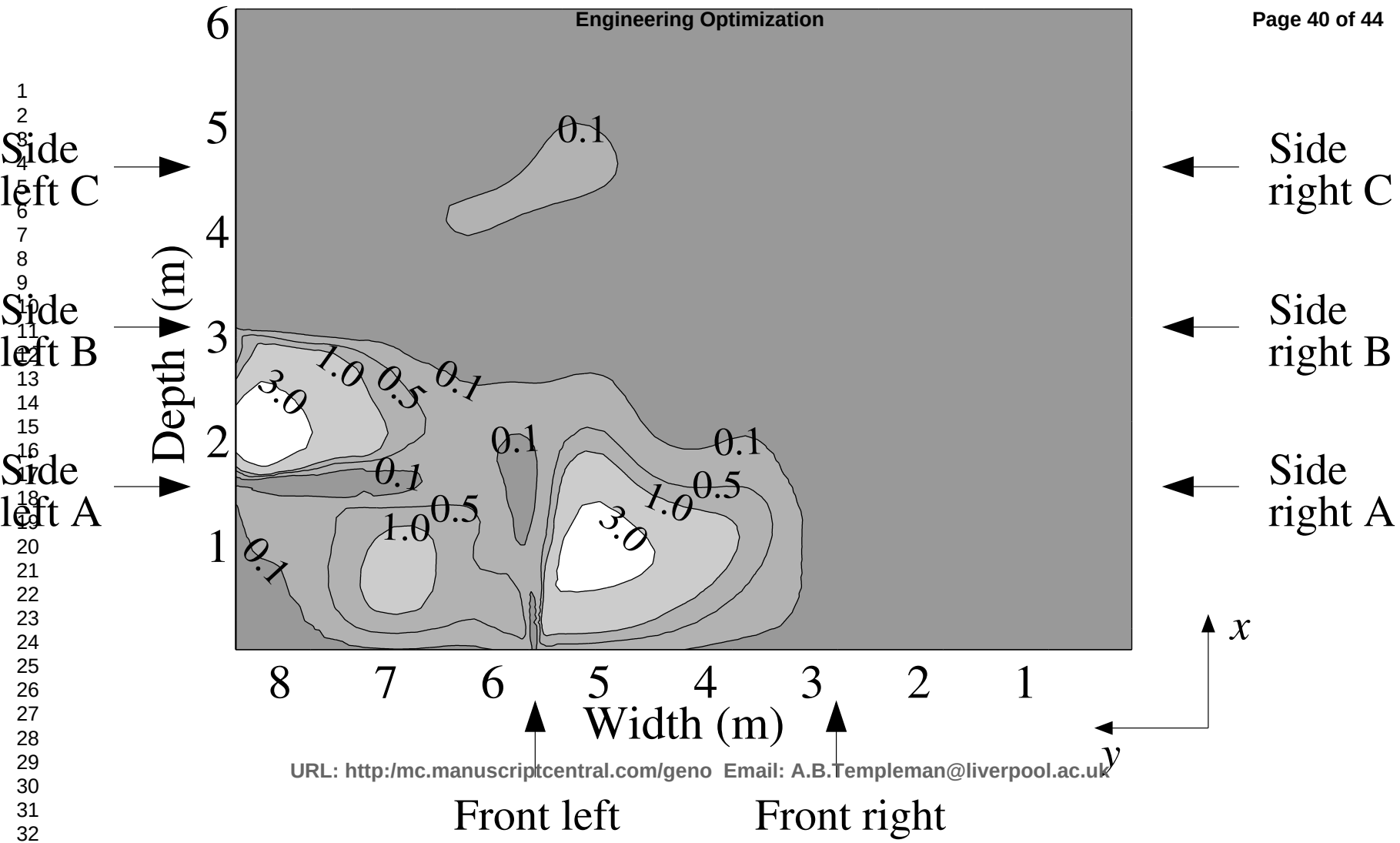
Side left C
Side left B
Side left A
Side right C
Side right B
Side right A
Depth (m)
Width (m)
Front left
Front right
x
y
0.1
1.0
0.5
3.0

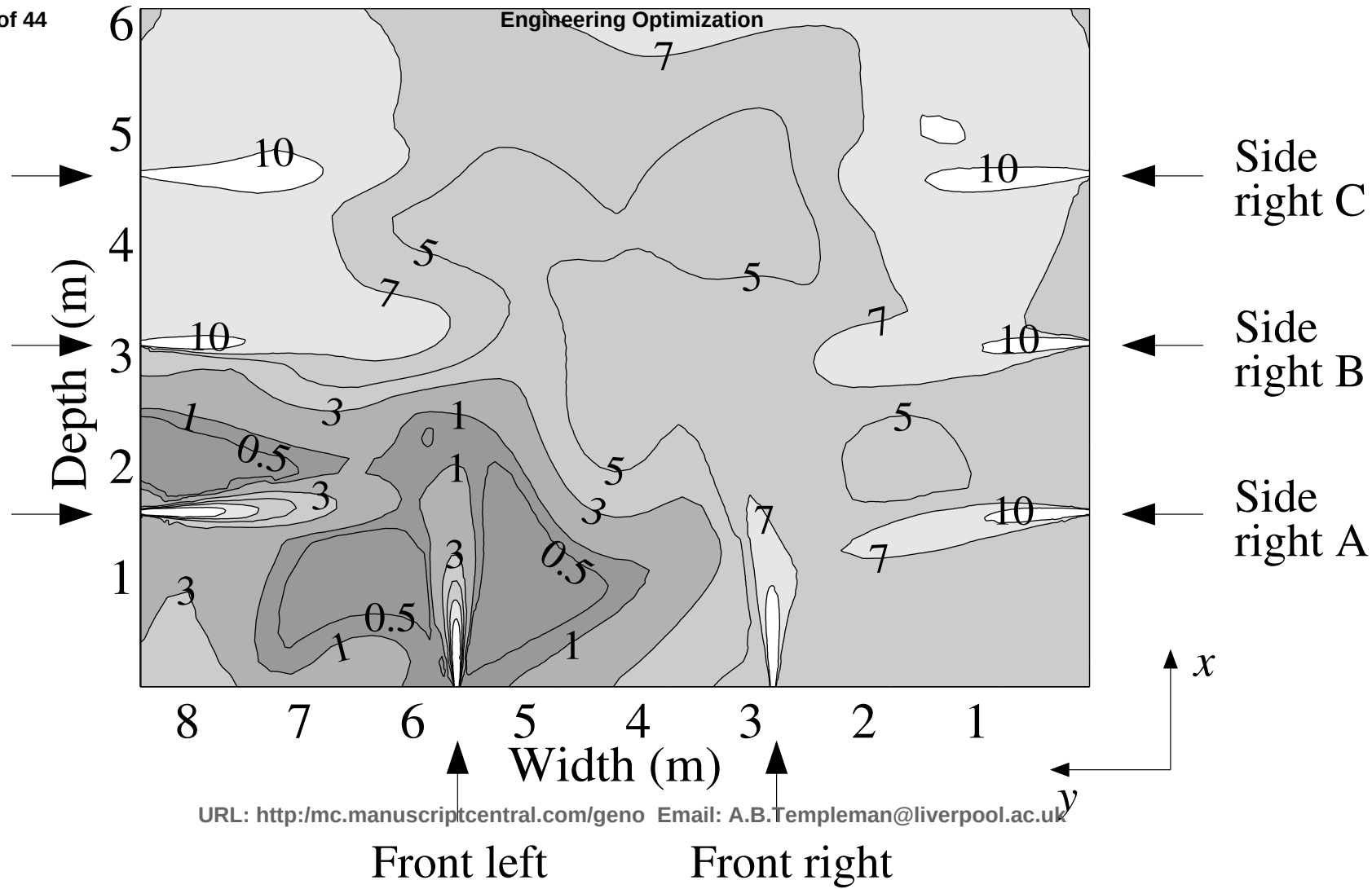
Side left C
Side left B
Side left A
Depth (m)
6
5
4
3
2
1
10
7
5
3
1
0.5
Side right C
Side right B
Side right A
8 7 6 5 4 3 2 1
Width (m)
x
y
Front left
Front right

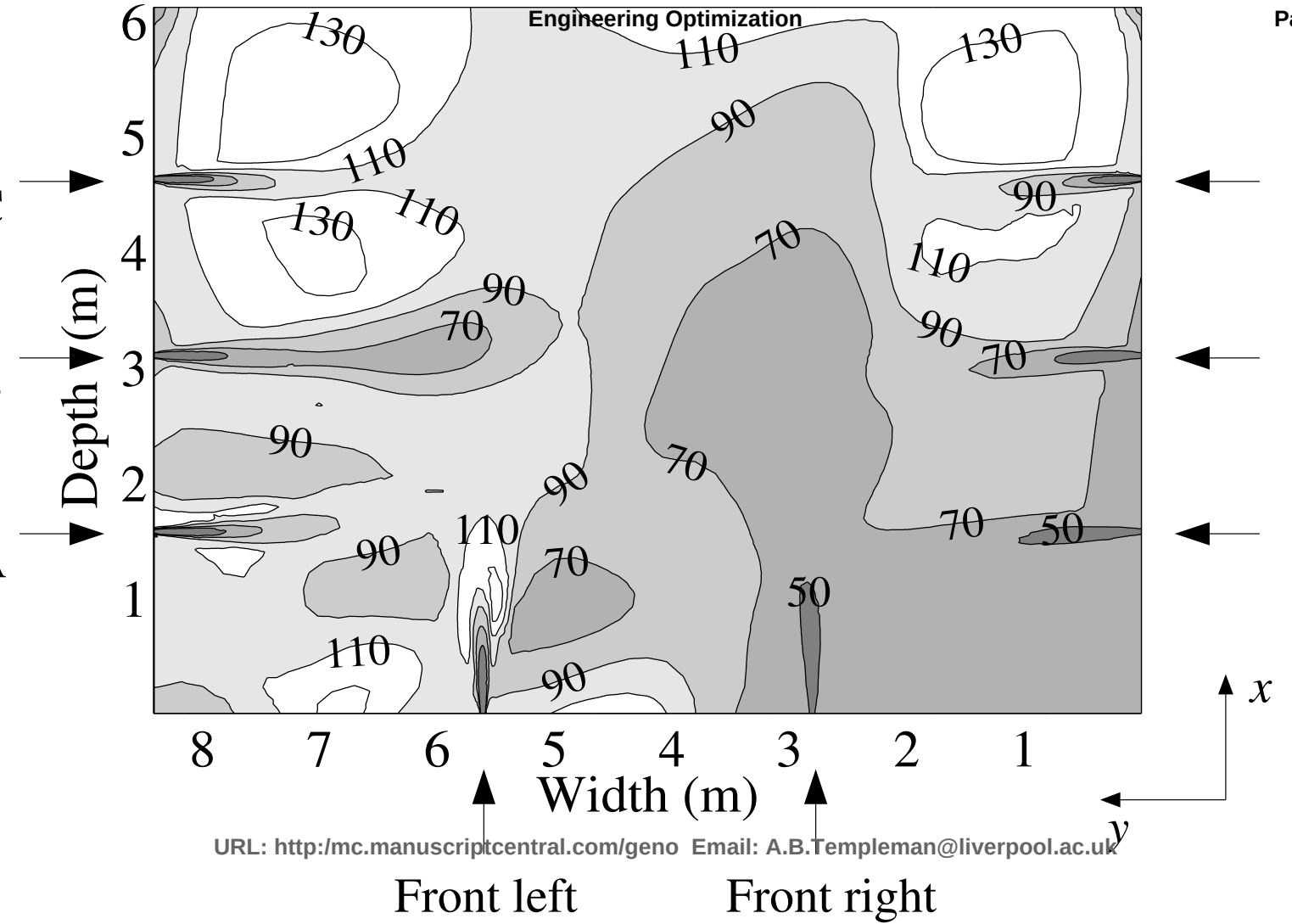
Side left C
Side left B
Side left A
Depth (m)
6
5
4
3
2
1
130
110
90
70
50
Side right C
Side right B
Side right A
8 7 6 5 4 3 2 1
Width (m)
x
y
Front left
Front right

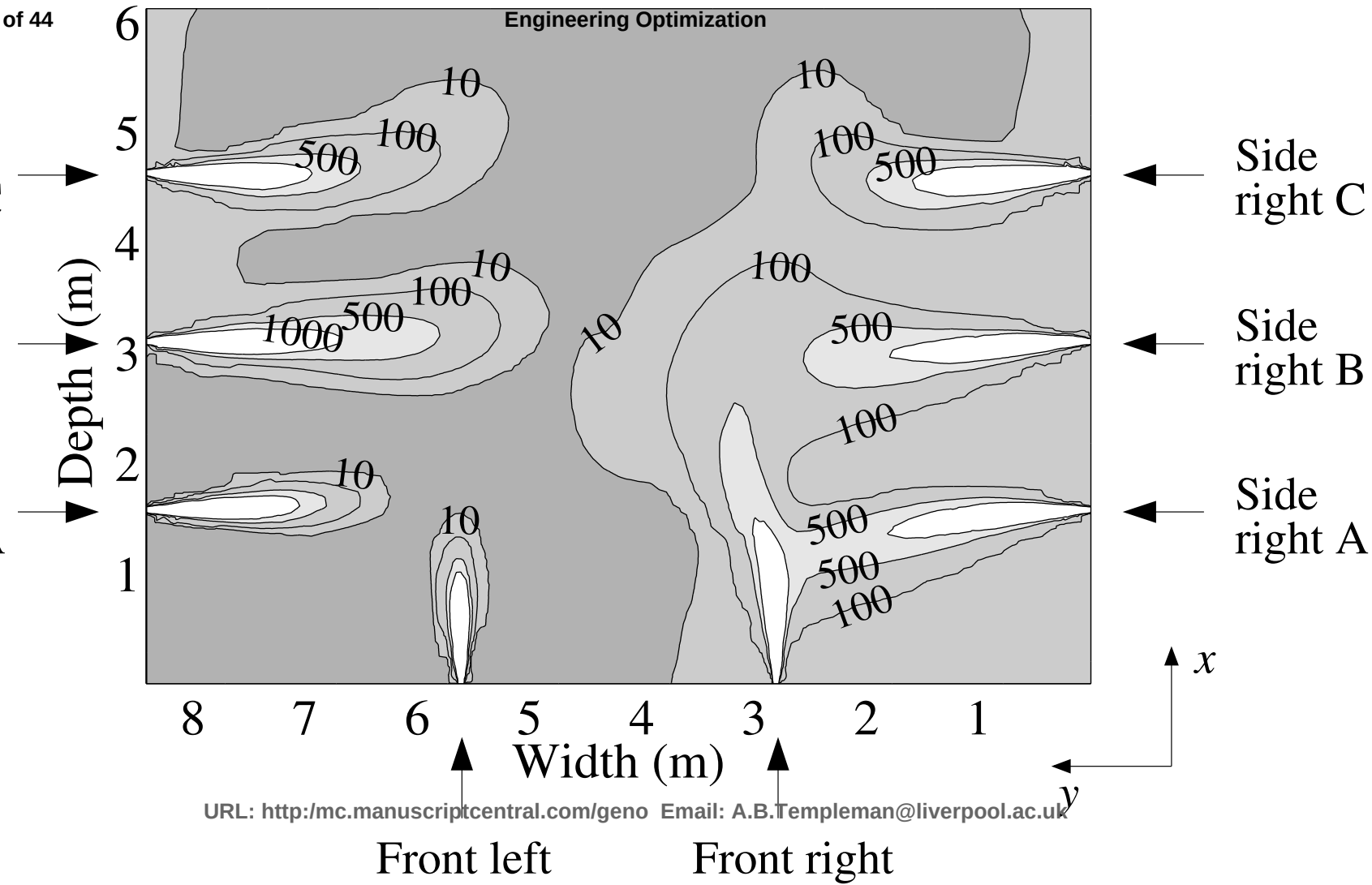
Side left C
Side left B
Side left A
Depth (m)
6
5
4
3
2
1
10
100
500
1000
Side right C
Side right B
Side right A
8 7 6 5 4 3 2 1
Width (m)
x
y
Front left
Front right

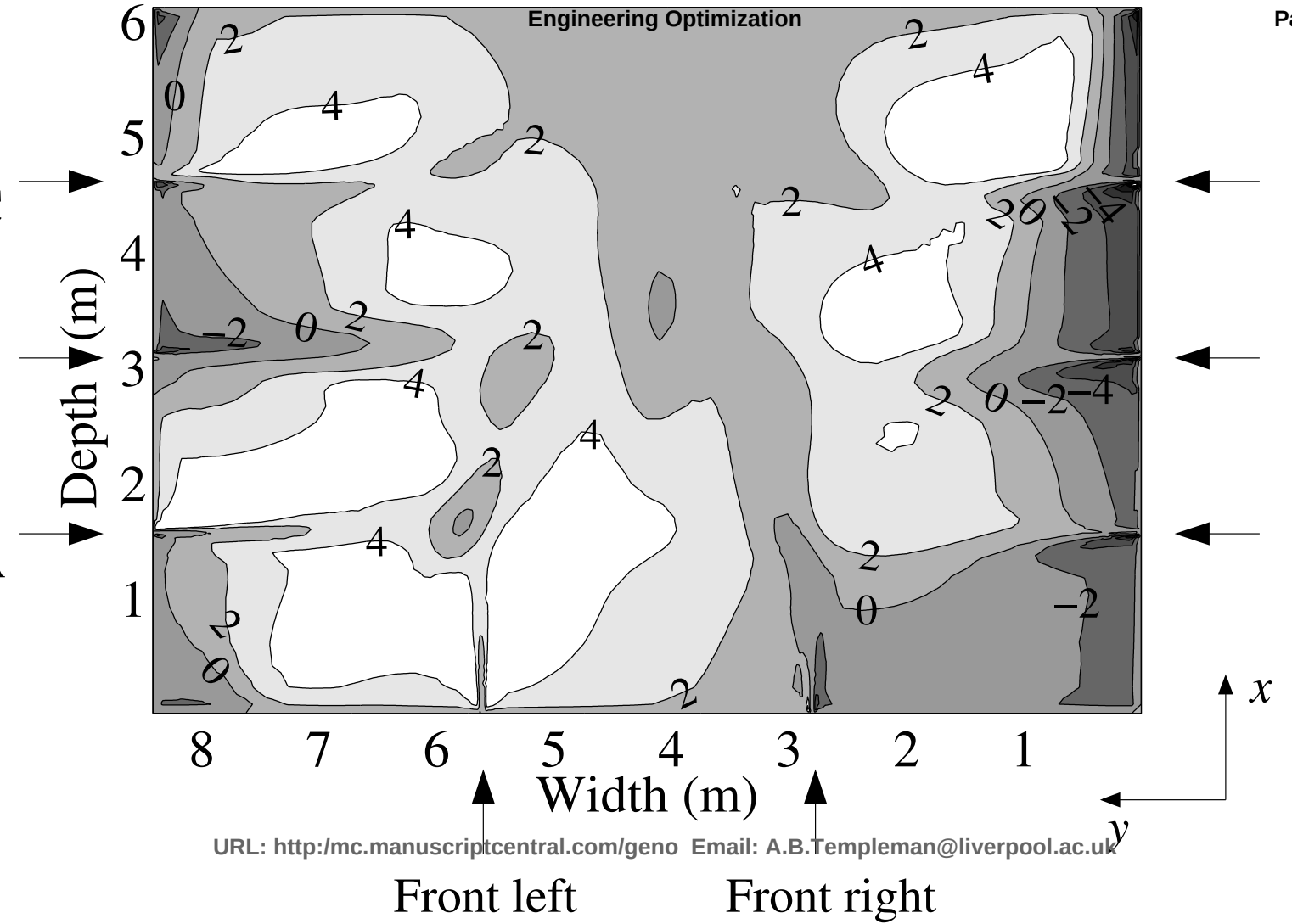
Side left C
Side left B
Side left A
Side right C
Side right B
Side right A
Depth (m)
Width (m)
Front left
Front right
x
y

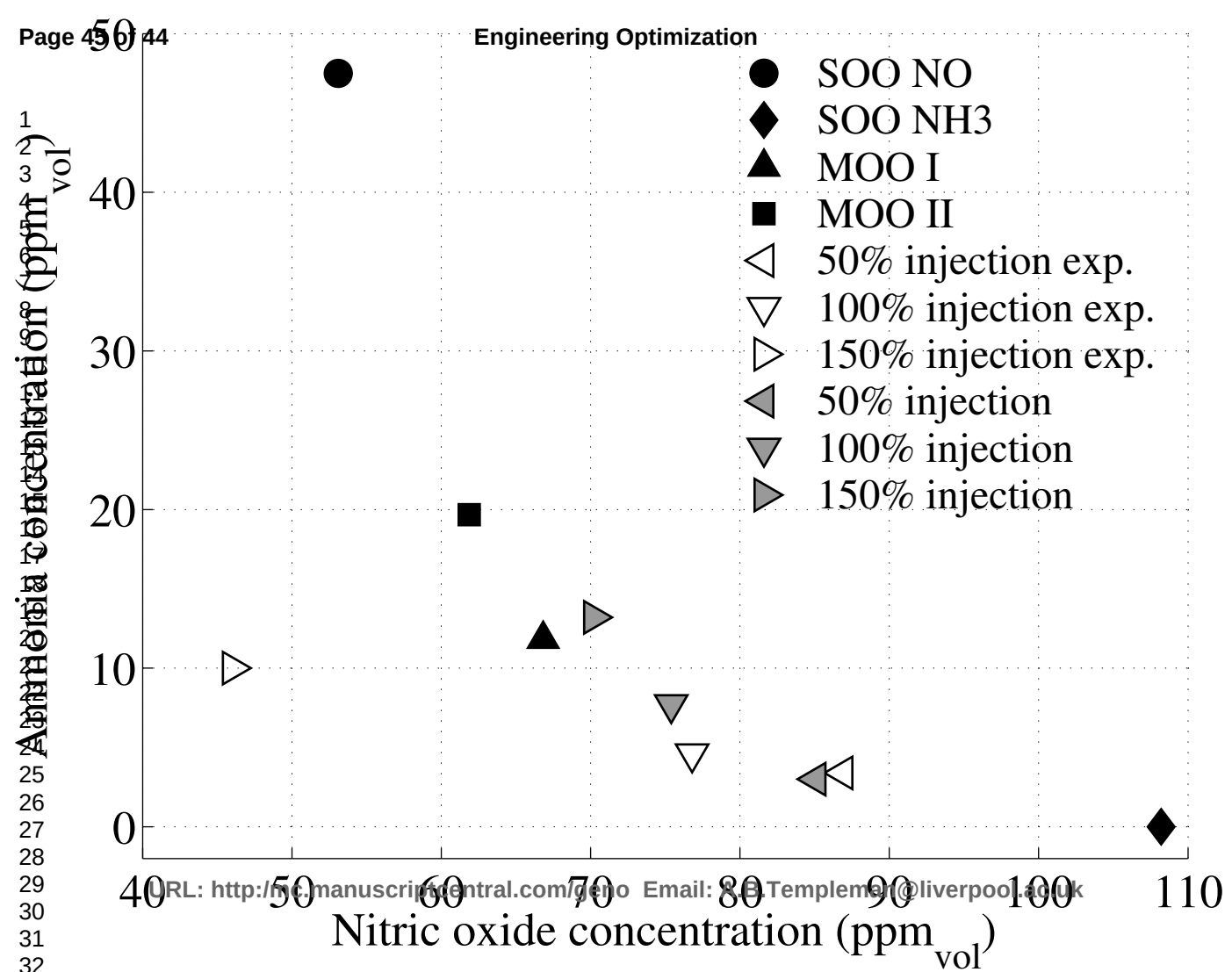
SOO NO
SOO NH3
MOO I
MOO II
50% injection exp.
100% injection exp.
150% injection exp.
50% injection
100% injection
150% injection
Ammonia concentration (ppm vol)
Nitric oxide concentration (ppm vol)
0
10
20
30
40
50
40
50
60
70
80
90
100
110